UNIVERSITY OF NAIROBI

ASSESSMENT OF FLOOD SUSCEPTIBILITY IN MOUNT ELGON REGION OF UGANDA UNDER A CHANGING CLIMATE AND RISK IMPLICATION TO FARMLAND FOOD SECURITY

OKAU PATRICIA

I56/40875/2021

A Dissertation Submitted in Partial Fulfillment of the Requirements for the award of the Degree of Master of Science in Meteorology of the University of Nairobi

November, 2023

DECLARATION

I declare that this dissertation is my original work and has not been submitted elsewhere for Examination, award of a degree or publication where other people's work or my work has been used, this has properly been acknowledged and referenced in accordance with the University of Nairobi's requirements.

Okau Patricia **Signature** _____ **Date** 06/12/2023
I56/40875/2021
Department of Earth and climate science
Faculty of Science and Technology
University of Nairobi

This dissertation is submitted for examination with our approval as University supervisors:

Prof. Alfred Owuor Opere **Signature** _____ **Date** 07/12/2023
Department of Earth and Climate Science
University of Nairobi
P.O Box 30197-00100
Nairobi Kenya
aopere@uonbi.ac.ke

Dr. Stephen K. Rwigi **Signature** _____ **Date** 07/12/2023
Department of Earth and Climate Science
University of Nairobi
P.O Box 30197-00100
Nairobi Kenya
rwigik@uonbi.ac.ke

DEDICATION

This work is dedicated to my family and friends.

ACKNOWLEDGEMENT

I express my gratitude to Almighty God for the wisdom, knowledge, and understanding bestowed upon me throughout the duration of my academic journey at the University of Nairobi.

I extend my heartfelt gratitude to my esteemed supervisors and mentors, Professor Alfred Owuor Opere and Dr. Stephen K. Rwigi. Your exceptional knowledge, patience and dedication to excellence have been instrumental in guiding me through this journey of academic growth and success.

Finally, I thank IGAD Climate Prediction and Application Centre (ICPAC) for awarding me the scholarship to pursue further studies at the University of Nairobi as well as financial support and mentorship throughout the study.

ABSTRACT

Climate extremes, specifically floods, have posed significant challenges to several regions of the world. Mount Elgon in particular experiences severe flood and its' impacts have drastically affected the region. Climate data used included the monthly observed data blended with Climate Hazards Group Infrared Precipitation with Station data (CHIRPS) for the period from 1991 to 2022 and climate change projections for scenarios under Representative Concentration Pathways (RCP) 2.6, RCP 4.5, and RCP 8.5 from the IGAD Climate Prediction and Application Centre (ICPAC) website. Rainfall trends from the Mann Kendall trend test varied across the seasons, with significant increases in Kapchorwa and Bukwo during the MAM season and uniform trends of intensified rainfall in the SON season while JJA and DJF season exhibited a non-significant increase in rainfall. To analyze flood susceptibility, the Analytical Hierarchy Process (AHP) model reveled rainfall, proximity to rivers, topography and land Use Land Cover as the most flood influencing factors and the weighted overlay integration generated a flood susceptibility map, revealing varying vulnerability levels of moderate to high with an area of 821 Sq.km and 1.6 Sq.km respectively. Furthermore, the study projects increased flood susceptibility in the region under scenarios Representative Concertation Pathways (RCP) 2.6, 4.5, and 8.5 emphasizing an escalating trend in flood susceptible areas, particularly in the northern region. The assessment of potential consequences indicates heightened flood risks in farmlands, particularly in Bukwo district, posing threats to agricultural activities and food production. These findings provide valuable insights into flood susceptibility dynamics and potential consequences considering changing climate condition. The findings underscore the need for proactive measures and adaptive strategies to address the increasing challenges posed by heightened flood risks. These measures are crucial for ensuring environmental resilience and promoting sustainable development in the Mount Elgon region.

Key Words: Flooding, Flood susceptibility, Climate projections, Farmland Food security

Table of Contents

LIST OF TABLES

LIST OF FIGURES

LIST ACRONYMS

AHP	Analytical Hierarchy Process
CA-ANN	Cellular Automata-Artificial Neural Network
CD	Climate Data
CDT	Climate Data Tools
CI	Consistency Index
CR	Consistency Ratio
DEM	Digital Elevation Model
DJF	December, January, February
FAO	Food and Agriculture Organization
GIS	Geographic Information System
ICAPC	IGAD Climate Prediction and Application Centre
IPCC	Intergovernmental Panel for Climate Change
JJA	June, July, August
LULC	Land Use Land Cover
MAM	March, April, May
MOLUSCE	Modules for Land Use Change Evaluation
OLI	Operational Land Image
RCP	Representative Concentration Pathways
RI	Random Index
SON	September, October, November
TWI	Topographic Wetness Index
UHI	Urban Heat Island
UNMA	Uganda National Meteorological Authority
USGS	United States Geological Survey

CHAPTER ONE

INTRODUCTION

1.1 Study Background

One of the most prevailing and noteworthy discussions in the field of weather and climate revolves around extreme weather and climate events. These events increased in both occurrence of occurrence and severity globally (Eckstein et al., 2021; Ripple et al., 2021) with the primary concern being the devastating impacts evident both on human systems and disrupted sustainable development (Eckstein et al., 2021; Zhang et al., 2019). Globally, flooding is one of the major focus of this discussion mainly because of their severe potential for destruction. The World Bank report of 2021 estimates a 1-in-100-year flood event, and more than one-fifth of the world's population is exposed to flood depths exceeding 0.12 m (El-Haddad et al., 2021; Rentschler et al., 2022). Recently, significant evidence has accumulated showing an increase in the occurrence and strength of floods, as well as threats to the well-being of people (Duan et al., 2022; Tabari, 2020).

The population exposed and affected by floods has skyrocketed in the past decade with an average of 90,000 deaths annually and about $40 billion in damages (UNFCC, 2021). In Africa, several studies clearly demonstrate that low-income communities as well as areas with limited capacity to cope are the most vulnerable to floods (Di Baldassarre et al., 2010). Additionally, floods have significant negative impacts on public health, food security, and consequently on development (Di Baldassarre et al., 2010). According to the World Bank, the economic cost of floods in Africa by 2010 was estimated to be around $3.4 billion per year, and this figure is projected to rise to $7 billion per year by 2025, and adaptation costs are projected to be about $15 billion by 2040-49 (Ciscar et al., 2010).

Uganda is among the low developed countries in Africa. It is recognized as one of the most vulnerable to flooding in Africa (WBG, 2021). Flooding is recognized as one of the deadliest natural disasters in the third National Development Plan (NDP) of the country, with flash floods and slow-onset floods commonly observed in the lowlands and along river banks (WBG, 2021). The highest impact of these floods is experienced among low-income communities; one such area is the Elgon region located in the Eastern side of Uganda (Jiang et al., 2014). This region is known for its diverse agricultural production, and numerous socioeconomic activities that depend on natural resources (Jiang et al., 2014).

Research in this field of extreme events has evolved as the significance of hazards' impacts to social, monetary, and ecological aspect continues to gain acknowledgement (Buchecker et al., 2013; Duan et al., 2022; Rentschler et al.,2022). Other scholars have focused on the efficiency of various measures aimed at mitigating and adapting to floods, such as structural and non-structural measures, community-based approaches, and land use planning. Despite this, these studies have largely neglected the specific context of Uganda, yet the increasing influence of increased precipitation due to climate change on floods is anticipated to have substantial implications to the food security of the local community who rely on farmlands as a source of food (Kansiime et al., 2013a; Resilience, 2010). Many vulnerable communities in the Elgon lowlands remain unprepared for the current and projected increase in flood frequency and intensity, posing significant risks to food security (Crawford et al., 2016).

While the study area has long recognized floods as one of the most destructive extreme event, recent research indicates that rising precipitation levels are expected to further escalate the frequency of flooding incidents (Rentschler et al., 2022). Therefore, it is fundamental to consider the potential influence of increased precipitation on floods and the associated impacts. Considering this background, the primary goal of this study was to examine the susceptibility in Uganda's most vulnerable region, the Elgon region, and the potential impact on farmland food security.

The study considers the definition of flood susceptibility by the Intergovernmental Panel on Climate Change (IPCC), which states that flood susceptibility is the probability or chance of an area being flooded, considering both the natural hazards and the vulnerability of the exposed elements (IPCC, 2021). This study identified areas prone to flooding and quantified the degree of susceptibility using Geographic Information System (GIS) and Analytical Hierarchy Process (AHP) methods to help Uganda develop effective preparedness and mitigation measures to tackle the potential risks related to projected flooding.

This study contributes to the evolving research on flood risk assessment, encompassing societal, economic, and ecological dimensions. It seeks to aid policymakers and stakeholders by identifying and prioritizing areas for effective early warning system development and strategies to mitigate and adapt to flood hazards, particularly in vulnerable communities in Uganda.

1.2 Problem Statement

Floods pose a persistent challenge globally, impacting infrastructure and threatening lives and livelihoods (O'Donnell & Thorne, 2020; Balgah et al., 2023). The Mount Elgon region in Uganda faces escalating flood occurrences due to a changing climate (WBG, 2021).

While existing studies identify major factors contributing to floods in the region, there's a gap in comprehensively mapping the areas at prone to flooding in the region, both current and projected. Despite global recognition of floods' impacts, the Mount Elgon region lacks specific research addressing its impacts specifically to farmlands food security yet the communities rely on rain-fed rain fed agriculture to achieve food security (Weldegebriel & Amphune, 2017).

Hence, the objective of this study is to address this gap by providing a synthesized map of flood-prone areas, current and projected, to guide tailored mitigation strategies, ensuring the region's resilience and sustaining rain-fed agriculture, vital for Uganda's economy.

1.3 Objectives

General Objective

The general objective of this study was to assess the flood susceptibility of the Elgon region of Uganda under a changing climate and risk implications to the farmland food security.

The research questions are:

1. What are the seasonal precipitation patterns changed in the Elgon region of Uganda?
2. What is the current spatial distribution of the flood-prone areas in the Elgon region of Uganda?
3. Which areas in the Elgon region will be prone to flooding in the future?
4. What are the impacts of projected floods to farmlands food security of communities living in the Elgon region?

1.3.3 Specific objectives

1. To examine the seasonal precipitation patterns in the Mount Elgon region of Uganda.
2. To determine the spatial distribution of current flood susceptibility of the study region.
3. To predict and map future flood susceptible areas of the study region.

4. To determine the impacts of the projected floods on of farmland food security in the region.

1.4 Justification and Significance

The effects of climate change are becoming increasingly evident, resulting in changes to weather patterns, altered precipitation, and an increase in floods. Understanding these changes is vital to develop effective strategies for adaptation and mitigation.

The study therefore fills crucial knowledge gaps by providing comprehensive data on flood susceptibility and changing precipitation patterns in the region. Through mapping both current and future flood-prone areas, it aids in risk assessment and preparedness, equipping communities with valuable information to bolster their resilience.

Furthermore, food security is a paramount concern for the communities residing in the Mount Elgon region. Flooding has the potential to disrupt agricultural activities, resulting in crop loss and food shortages. Investigating how floods affect farmland food security is not only academically significant but also directly impacts the well-being of local populations in order to maintaining a secure food supply in the face of climate change impacts.

CHAPTER TWO

LITERATURE REVIEW

2.1 Introduction

This chapter presents a synthesis of past studies that have explored flood susceptibility, methods used for the assessment, flood conditioning factors, how climate change is affecting flood-prone areas and the implications of projected flood susceptibility on farmland food security globally, regionally and locally.

2.2 Flood Susceptibility Assessment

As discussed in section 1.1, flood susceptibility is the probability or chance of an area being flooded, considering both the natural hazards and the vulnerability of the exposed elements similarity, flood susceptibility assessment involves evaluating the likelihood of an area to experience flooding.

Flood susceptibility assessment is significant towards effective flood risk management technique (Milly et al., 2002; Rentschler et al., 2022). Over several years, studies have been done to investigate flood susceptibility in various regions globally.(Di Baldassarre et al., 2010; Ekeanyanwu et al., 2022; Karmakar et al., 2010; Umaru & Adedokun, 2020; Ward et al., 2013; Wright, 1994; Zehra & Afsar, 2016).

Most of these studies have utilized various techniques such as hydrological modelling, remote sensing, and Geographic Information System (GIS) to detect areas prone to flooding (Wright, 1994). While hydrological models and Geographic Information System (GIS) have been widely used to study flood susceptibility, some critics argue that they have limitations in accurately predicting floods and their impacts on agricultural systems (Wright, 1994). One limitation is that hydrological models rely heavily on data inputs, which may be subject to errors and uncertainties. Additionally, the efficiency of hydrological models is highly reliant on the quality and availability of the contribution data needed to develop the model, which may not always be reliable or consistent across different regions or periods (Albano & Sole, 2018).

2.3 Flood conditioning factors

In an attempt to gain understanding of flood susceptibility, most studies used GIS to integrate various flood influencing factors. These factors are referred to as conditioning factor (Forte et al., 2006). (Edamo et al., 2022; El-Haddad et al., 2021; Pourali et al., 2016) demonstrated that places with a high Topographic Wetness Index (TWI) are more prone to flooding during heavy rainfall events, emphasizing the significant influence of TWI on flood occurrence.

Similarly, Ogania et al., (2019) and Rocha et al., (2020) studied the effect of elevation and slope and found that higher elevation and slope translated to lower probability of flooding and lower elevation translated to higher probability of flooding. It directly impacts the speed of surface water runoff and consequently infiltration rate (Rocha et al., 2020). Slopes have a negative influence on infiltration and a positive influence on the velocity of runoff, hence high flooding, and the gentle slopes have a positive influence on infiltration and a negative influence on runoff velocity hence low flooding (Samanta et al., 2018).

For precipitation, (Chen et al., 2022; Edamo et al., 2022; Ekeanyanwu et al., 2022; Kim et al., 2019) show that precipitation has an inverse relationship with the probability of flooding and that this is a very essential factor in flood proneness analysis and modeling. This factor is considered as the primary and significant cause of floods (Rahman et al., 2021; Yamazaki et al., 2018). Extreme rainfall is positively correlated to flood occurrences (O'Donnell & Thorne, 2020). Higher rainfall rates considerably increase the probability to flood and lower precipitation rate decrease the probability to flood (Edamo et al., 2022).

Land Use Land Cover(LULC) and Normalized Difference Vegetation Index (NDVI) influence flooding by affecting the amount of water runoff and infiltration in a given area (Adnan et al., 2020; Rahman et al., 2021; Samanta et al., 2018). Land use land cover (LULC) was considered since it influences flooding through the hydrological parameters of runoff and infiltration as well as being an element that signifies the present condition of the land, its configuration, and category, along with its significance regarding soil steadiness (Akdeniz et al., 2023; Tariq et al., 2022). Areas with vegetation slow down run-off and a have high infiltration rate, reducing the probability of flood whereas built-up areas have a low infiltration rate, thereby increasing the probability of flood (Costache, 2020).

Similarly, previous studies have examined the influence of proximity to the river and road on flooding (Adnan et al., 2020; Karmakar et al., 2010; Rahman et al., 2021). The proximity to the

road and the river are important factors in flood mapping because they significantly affect the amount of water that reaches a particular location during a flood event. Studies have shown that the closeness of a location to a river or stream increases the likelihood of flooding (Janizadeh et al., 2019; Samanta et al., 2018; Tariq et al., 2022). Proximity to the road influences flood susceptibility. Roads and other impervious surfaces can increase the speed and volume of surface runoff during heavy rainfall events, which can result in localized flooding in low-lying areas(Albano & Sole, 2018; Samanta et al., 2018; Tariq et al., 2022).

Edamo et al., (2022) and Tariq et al., (2022) showed that drainage density reflects the amount of water that can be accumulated in a particular area during a rainfall event by controlling the runoff and infiltration rate. Areas with higher drainage density tend to have more channels and tributaries, which can facilitate the flow of water and reduce the likelihood of flooding. On the other hand, areas with low drainage density are more likely to have less flow capacity, leading to water accumulation and flooding during heavy rainfall.

And finally, the variable that is input into ArcGIS to accurately study the flood susceptibility of a place is soil type. Soil type is a crucial variable for accurately assessing flood susceptibility in ArcGIS. Studies by (Edamo et al., 2022; Janizadeh et al., 2019; Karmakar et al., 2010; Montz & Evans, 2001) have highlighted that reduced soil water absorption capacity leads to increased water runoff, elevating the likelihood to flood. The influence of soil on the infiltration rate and surface run-off is a significant factor that influences flooding. Coarse–textured soils have larger pore spaces and hence higher rates of infiltration, which in turn reduces flooding and the same is the opposite for fine-textured soils (Karmakar et al., 2010).

2. 4 Climate Change and Flood Susceptibility

Changes in climate have increased variations in the occurrence and strength of floods in most regions of the world as flood susceptibility and extreme rainfall are directly proportional (IPCC, 2021). Extensive evidence indicates that global climate changes are anticipated to result in increased precipitation, thereby altering flood-prone areas worldwide.(Chen et al., 2022; Crawford et al., 2016; Dankers & Feyen, 2009; Duan et al., 2022; Karmakar et al., 2010; Kim et al., 2019; Zbigniew W. Kundzewicz et al., 2014; McKinney & Wright, 2021; Milly et al., 2002; Onyutha et al., 2021; Papalexiou & Montanari, 2019; Simonović, 2009; Tabari, 2020; Yamazaki et al., 2018). These studies have used various methods, including “global flood risk models, statistical analyses,

and hydrological approaches", to comprehensively scrutinize the influence of climate change precisely variations in precipitation and temperature patterns on flood-prone areas in various regions.

Yamazaki et al., (2018) studied a worldwide flood risk model that incorporates the effects of climate change. The study showed that the impacts of climate change are anticipated to result in an elevated flood hazard and risk across multiple regions. Notably, the research underscored that this escalation is particularly pronounced in Asia. They also note that adaptation measures, such as improved flood protection infrastructure, may be necessary to alleviate the climate change impacts. Similarly, Tabari (2020) investigated the connection of extreme rainfall, flood events, and climate change. The study found that "there is a potential for an escalation in extreme rainfall and flood events across all climate zones. The magnitude of this increase is mainly distinct in regions categorized by higher levels of rainfall".

Onyutha et al., (2021) studied how climate change will affect rainfall and evaporation in different parts of Uganda. They found that both rainfall and evaporation will generally increase across Uganda, but the changes will vary from place to place. The eastern part of Uganda will get more rain. These changes will have important implications on water resources in Uganda, so it is important for people to plan and prepare for them.

Di Baldassarre et al., (2010) reported that topography, land use changes and precipitations as the major factors that cause the floods in the region. However, the major factor of increased occurrence and strength of floods in this region are the result of increased altered precipitation patterns caused by a complex interplay of global and regional drivers, such as ENSO, IOD and the equatorial rain band oscillation (Ngoma et al., 2021) as well as local driver such as LULC changes, deforestation, and soil degradation (Jiang et al., 2014; Kansiime et al., 2013b).

2.5 Implication of Projected Flood Susceptibility on Farmland Food Security

Food security is one of the utmost discussed topics during and after flood events because of its direct negative influence on crop production particularly in the developing countries (Reed et al., 2022; Week & Wizor, 2020). The concept of food security is complex. The World Food Summit, as outlined by Shaw, (2007), described food security as the condition where individuals consistently possess the physical and economic means to acquire an ample supply of safe, nourishing food that aligns with their dietary requirements and preferences, promoting an active

and healthy lifestyle. This characterization of food security includes the scopes of food availability, food accessibility, and food utilization

In Mount Elgon region however, it is crucial to emphasize that the indigenous people rely on agricultural yields from the farmlands for their food and economic benefit (Uganda Investment Authority, 2019), FAO argues that the kind of food insecurity where there is temporary food shortages resulting from climate-related hazards like floods is defined as "transitory food security" (Pinstrup-Andersen, 2009; Uribe, Álvarez et al., 2010). The world bank on the other hand suggest that the term "farmland food security" should be used to define the state in which agricultural lands and farming systems within a region or community can consistently and sustainably produce an adequate quantity and quality nutritious food that satisfies the dietary requirements and food choices for a healthy lifestyle (Fischer & Shah, 2010), Therefore, this study adopted to investigate the implication of projected flood susceptibility on "farmlands food security".

Farmland food security aims to guarantee that the local community has reliable access to safe and nutritious food sources, reducing the risk of hunger, malnutrition and food-related crisis (Fischer & Shah, 2010). However, agricultural activities in this region rely on good climate conditions to thrive yet climate change/variability has been recognized as the major contributing factor for the decline and uncertainty the agricultural sector (Balgah et al., 2023; Gitz et al., 2016;; SHIFIDI, 2016; Simonović, 2009; Weldegebriel & Amphune, 2017). The intricate relationship between floods and crop production presents a potential risk of diminishing crop yields, crop losses and reduced productivity, soil degradation and nutrient leaching hence vulnerable populations face exacerbated food insecurity stemming from limited food access.

Several studies examined the risk implications of floods to food security across different geographical locations globally (Balgah et al., 2023; G.Ramakrishna et al., 2014; SHIFIDI, 2016; Week & Wizor, 2020; Duan et al., 2022; Resilience, 2010) and that floods have a severe impact on agriculture, destroying crops, washing away fertile soil, and contaminating water sources. This leads to a decline in agricultural productivity, food insecurity, and increased poverty. The impact of floods on agriculture is expected to become more severe due to the changing climate. However, none of these studies have focused on the Elgon region of Uganda. This presents a gap which this study seeks to fill.

2.6 Conceptual framework

This study was grounded on the fundamental concepts of impact-based forecasting. This concept evaluates changes in one independent variable (climate change) and the relationship to a dependent variable (floods) and consequently the impact on another dependent variable (food security) among communities in the region of study.

Climate was conceptualized as an independent variable that includes climate variables such as rainfall and frequency and harshness of extreme climate events. These climate stressors are bound to result in increased flooding in the Elgon region.

Flood susceptibility was conceptualized as a dependent variable, which is caused by conditioning factors such as extreme rainfall events, soil type, slope, LULC, distance to rivers and roads, NDVI, elevation, and drainage density. The increased flood susceptibility of the Elgon region would likely increase likelihood of food security of the people living in the region.

The variable of farmland food security was theorized as a dependent variable that is influenced by flooding resulting from increased flood susceptibility caused by increased precipitation. Floods presents a potential risk of diminishing crop yields, crop losses and reduced productivity, soil degradation and nutrient leaching hence exacerbate food insecurity among vulnerable population in the Mount Elgon region.

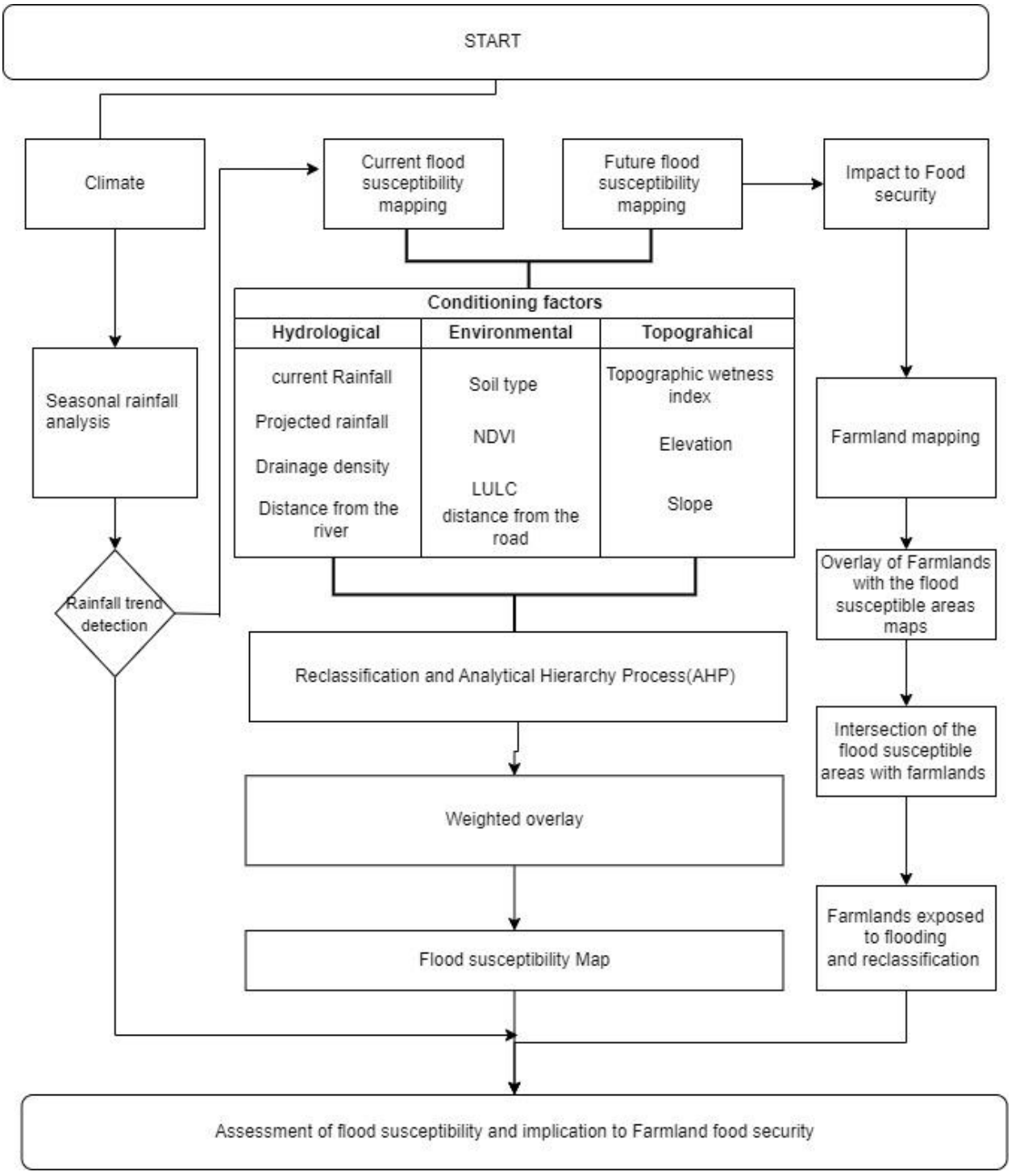

Figure 1: Conceptual frame work (A GIS-based IBF model modified from the Uganda Risk and Vulnerability Atlas, (OPM, 2020))

CHAPTER THREE

DATA AND METHODOLOGY

3.1 Introduction

This chapter presents the data types and sources that were used in the study, detailed overview of the study area and its biophysical characteristics. The chapter also presents the methods that were used for data collection and analysis used to achieve the study objectives.

3.2 Area of study

This Study was conducted over Elgon region of Uganda. This region lies North of the equator in the Eastern part of Uganda within latitude 0.5383N to 1.6614N and longitude 34.0741E to 34.9915E (Figure 2). The region occupies an approximate total area of 4,000 square kilometers and comprises of 8 districts (Mbale, Sironko, Manafwa, Bududa, Bulambuli, Kapchorwa, Kween and Bukwo).

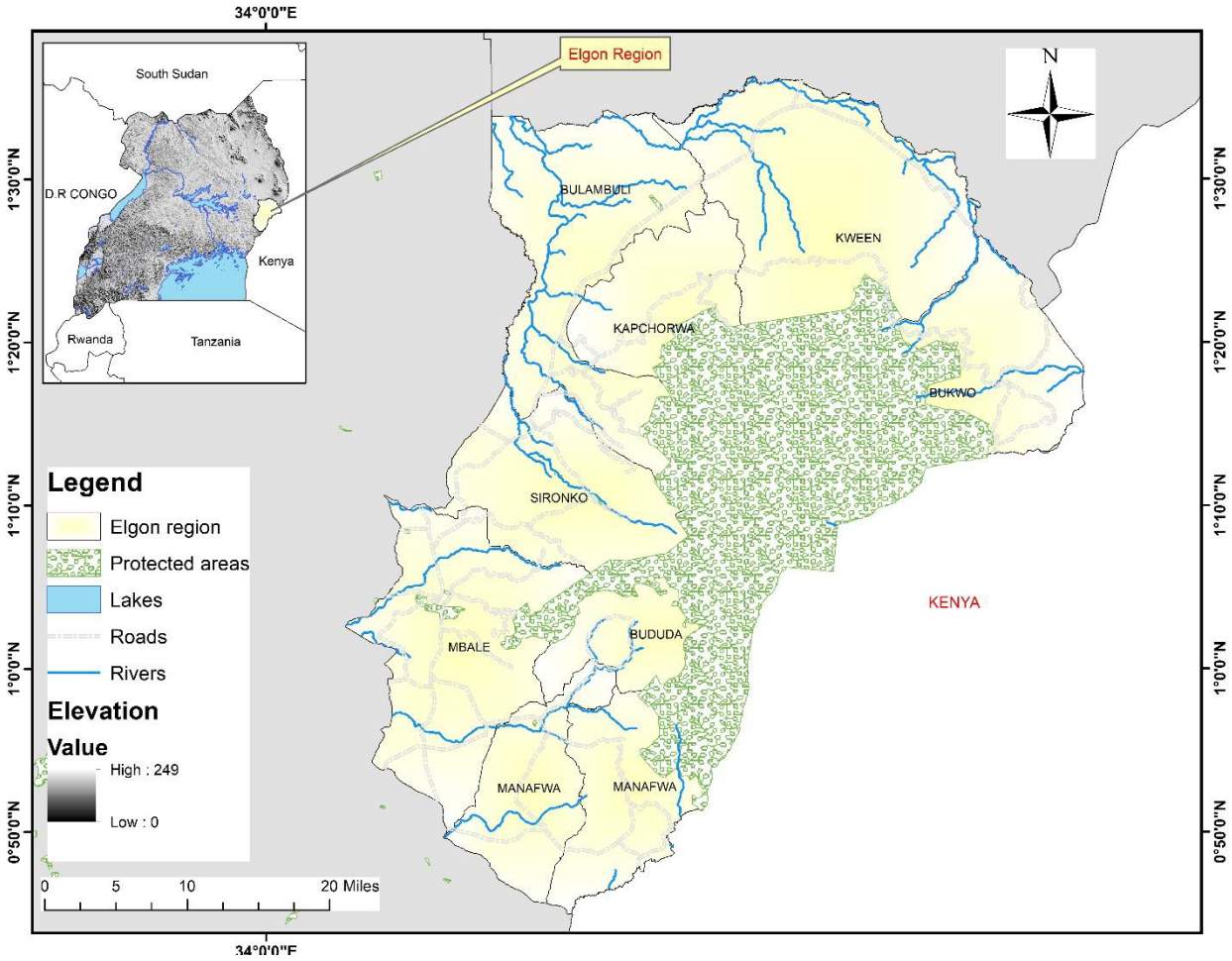

Figure 2: Study area map (shaded yellow) showing the rivers (blue), roads(grey) and protected areas(green) prepared in ArcGIS 10.5.

The region borders Kenya which can be accessed through Manafwa border post in Manafwa district and neighbors the Karamoja, Teso and Bukedi regions internally**.** The typographic feature located in this region is Elgon, this mountain is an inactive volcano and is the fourth-highest mountain in East Africa. Finally, the area is characterized by its significant elevation with the highest point reaching an altitude of 4,322 meters above sea level (Nakileza & Mugagga, 2022).

3.2.1 Climate of Mount Elgon Region

The region experiences bimodal rainfall patterns; long rains received in March, April and May (MAM) season followed by short rains in the September, October and November (SON) season. The region receives an estimated annual mean rainfall of about 1500 mm and the annual mean air temperature of about 23°C (Bonzemo, 2018). The climatology of the area of study relies deeply on the rainfall dynamics of Mount Elgon.

Rainfall distribution is influenced by several systems ranging from local to global drivers. The local drivers including the influence from the orographic lifting of moist air masses creating local microclimates due to the presence of Mount Elgon as well as the changes in the urban heat island due to changes in land cover resulting from deforestation, urbanization and agricultural activities.

Among the regional and global systems that influence the climate of the study are the Inter-Tropical Convergence Zone (ITCZ), Indian Ocean Dipole (IOD) and the East African Monsoon.

The Inter-tropical convergence zone is a major global driver of the rainy season in this region, this band of converging winds from both the Northern and Southern Hemispheres influences seasonal rainfall in the region of study.

This convergence zone shifts northward and southward with the changing seasons, bringing rainfall as it moves across the equatorial region. Over the Elgon region, the movement of the ITCZ is a critical factor in the onset and cessation of rainy seasons, influencing both the timing and duration of rainfall events (Lashkari & Jafari, 2021).

The Indian Ocean Dipole (IOD) is a sea-surface temperature anomaly in the Indian Ocean that affects weather and climate patterns in the surrounding regions. The IOD's positive phase is associated with warmer waters in the western Indian Ocean and cooler waters in the eastern Indian Ocean (Endris et al., 2019). This sea-surface temperature gradient influences atmospheric circulation patterns, impacting the Elgon region's rainfall. During a positive IOD phase, reduced moisture transport from the Indian Ocean can lead to decreased rainfall in the region, while a negative IOD phase may enhance rainfall (Endris et al., 2019).

The East African Monsoon is another significant climate system affecting rainfall patterns in the Elgon region. This monsoon is characterized by the seasonal reversal of winds, with moist maritime air from the Indian Ocean being drawn inland during the wet season. The monsoon's strength and directionality help in determining the amount of moisture transported over the region, impacting rainfall amounts. Research by Palmer et al., (2023) highlights the strong connection between the East African Monsoon and precipitation variability in the region, underscoring its influence on the Elgon region's rainfall patterns.

3.2.2 Population and economic activities

The region is home to a large population, with an estimated 3 million people residing within the eight districts (UBOS, 2020). Among the livelihood activities in the region include tourism and agriculture and 90% of this population relies on agriculture as a source of livelihood (Uganda Investment Authority, 2019). The most common land use type among built-up areas, bare land, and forest cover is agriculture(Uganda Investment Authority, 2019). The most common agricultural practice carried out in this area is subsistence farming both in the low land and mountain slopes (Uganda Investment Authority, 2019).

3.3 Data Types and Sources

The datasets that were used in this study included historical and downscaled projected rainfall data as well as raster datasets of the conditioning factors.

3.3.1 Rainfall Data

The rainfall datasets that were used in this study were obtained from two sources. First, the monthly observed data blended with CHIRPS data in Climate Data Tools (CDT) for six observation points across the Elgon region as shown in table 1 below for the period from 1991 to 2022 obtained from Uganda National Meteorological Authority (UNMA). Similar dataset has been used by (Obubu et al., 2021) to assess the recent changes in climate in the Lake Kyoga Basin of Uganda.

Table 1: Rainfall observation points used in the study and their coordinates

station	Latitude	longitude
Mbale	1.074773	34.17715
Bududa	1.025107	34.37093
Kapchorwa	1.397089	34.45075
Bunginyanya	1.2833	34.35
Bukwo	1.289369	34.73928
Sironko	1.229645	34.24803

Secondly, climate change projections from Regional Climate Model - Max Planck Institute(RCA-MPI) for the domain that covers longitude 21.84E TO 51.39E by 0.05 N=592pnts and 11.74N to latitude 22.91N by 0.05 N=694pnts based on the IPCC Representative Concertation Pathways; RCP 2.6, RCP 4.5 and RCP 8.5 (IPCC, 2014) downloaded from Intergovernmental Authority on Development Climate Prediction and Applications Centre (ICPAC) website were used. This data was subjected to processing in Climate Data Operators (CDO) where the period of 2030 to 2050 was cut, re-gridded using the CHIRPS' data layer to the Elgon region grid of latitude 0.5383N to 1.6614N and longitude 34.0741E to 34.9915E and finally units converted from kilogram per meter per second to millimeter per day.

3.3.2 Conditioning factors data

The flood susceptibility model utilized raster datasets acquired from various sources, as indicated in the table provided in table 2 below. Digital Elevation Model (DEM) was used to extract the information of the topographic influence on hydrology in the region to include the Topographic Wetness Index (TWI), slope, and elevation.

Table 2: Data sources and their resolution

No	Data	Data source	Output	Resolution
1	DEM	https://dwtkns.com/srtm30m/	elevation	30m
			slope	
			TWI	
2	LULC (Landsat 8 OLI)	https://earthexplorer.usgs.gov/	Land cover map	30m
3	Soil	NARO	Soil map	30m
4	Road Network	UNRA 2017/open street map	Proximity to the road	
5	Rivers	NFA 2015	Proximity to the rivers	
			Drainage density	
6	NDVI	https://earthexplorer.usgs.gov/	NDVI	30m

3.4 Methods of Data Analysis

This section describes the homogeneity test method, the methods employed to achieve the specific objectives of the study comprising of the examination of the seasonal precipitation patterns, determination of the spatial characteristics of current flood susceptibility, prediction and mapping of future flood susceptible areas, and determination of the impacts of the projected floods on the farmland food security.

3.4.1 Homogeneity Test

In this study, homogeneity testing was conducted using the single mass curve in R-software. This method involved plotting the cumulative climatological value of rainfall in millimeters against time in years. A study by Wakachala et al., (2015) as well utilized this method. A homogeneous data record was indicated by a straight line plot, while heterogeneity was indicated by evidence of shifts in the cumulative straight line plot due to mean shifts.

3.4.2 Examination of the Seasonal Temporal and Spatial Rainfall Patterns

In this study, the methods that were used to examine the temporal and spatial rainfall patterns over the specified period of 1991 – 2022 over the study area included statistical analysis of trends using the Mann-Kendall test and Sen's slope estimator (Adhikari et al., 2018). These methods were chosen because they are commonly used by researchers for trend analysis to show significant statistical trend time-series (Aditya et al., 2021). Furthermore, the methods do not rely on the normality assumption of data, they are robust against outliers and do not require the data to be evenly spaced (Adhikari et al., 2018; Alashan, 2020; Aswad et al., 2020; Roy & Chakravarty, 2021).

3.4.2.1 Mann-Kendall Test

This method was employed to identify trends in time sequence data (Aditya et al., 2021). It is based on the ranking of the data and computing a test statistic that H0 assumed no trend and H1assumed existence of a trend in the data. If the p-value was less than 0.05 which is the significance level, the H0 was rejected, and a trend was considered to be present and if the p-value

was greater than the significant level, then there was no trend in the data.(Adhikari et al., 2018; Roy & Chakravarty, 2021).

The Mann Kendall test was calculated using equation (1.0) which involved calculating the sum of all pairwise differences in the data points, taking into account the signs of the differences. The equation calculated all combinations of data j and k from 1 to (n-1) and k+1 to "n" values respectively within the sample, where "n" represents the length of the sample.

$$S = \sum_{j=1}^{n-1} \sum_{k=j+1}^{n} \text{sign}(x_j - x_i), \quad \text{sign}\,(xj - xi) = \begin{cases} +1, & \text{if } x_k - x_j > 0 \\ 0, & \text{if } x_k - x_j = 0 \\ -1, & \text{if } x_k - x_j < 0 \end{cases} \tag{1.0}$$

A positive S value indicates an upward trend of rainfall in the Mt. Elgon region, while a negative value indicated a downward trend of rainfall over the Mount Elgon region. The variance (S) of the rainfall was computed using equation 2.0 in order to obtain the Z values.

$$\text{Var}(S) = \frac{1}{18}\left\{ n(n-1)(2n+5) - \sum_{p=1}^{g} t_p\,(t_p - 1)(2t_p + 5) \right. \tag{2.0}$$

Where n denotes number of data points in the dataset, g denotes the number of tied groups and t_p denotes the number of data points in the pth group

A tied group (g) is a set of rainfall data with the same value when the sample size is n>10. A standardized measure of test statistics (Z), was determined using the equation (3.0).

$$Z = \begin{cases} \dfrac{S-1}{\sqrt{\text{Var}(S)}} & \text{if } S < 0 \\ 0 & \text{if } S = 0 \\ \dfrac{S+1}{\sqrt{\text{Var}(S)}} & \text{if } S > 0 \end{cases} \tag{3.0}$$

A positive value of Z indicated an increasing trend of rainfall over the Mount Elgon region. While a negative value of Z indicated a downward trend.

3.4.2.2 Sen's Slope Estimator

This method estimates the magnitude of the trend using a non-parametric method. (Aditya et al., 2021). The estimator calculates the magnitude of any trend found in the Mann-Kendall test slope of each pair of observations in the data and computes the median of all the slopes. (Adhikari et al., 2018; Alashan, 2020; Aswad et al., 2020; Roy & Chakravarty, 2021). Multiple estimates (N) were made of the slope using equation 4.0:

$$Q_{med} = \frac{x_j - x_i}{j - i}, i = 1,2,3, \dots, N \quad (4.0)$$

xj and xi denotes data values at time j and, respectively. If there are n values of xj in the time series, there will be N = n(n-1)/2 slope estimates. The N value of Qi is sorted from smallest to largest, then Sen's Slope used median Qi (Qmed). A two-tailed test estimated the value of Qmed at a confidence interval of 95% calculated using equation 5.0.

$$Q_{med} = \begin{cases} Q_{[(n+1)/2]}, & if\ n\ is\ odd \\ \frac{Q_{[n/2]} + Q_{[(n+2)/2]}}{2}, & if\ n\ is\ even \end{cases} \quad (5.0)$$

3.4.2.4 Spatial Analysis

In this study, Climate Data Tools (CDT), an R-based software package, developed by International research institute for climate and society (IRI) as part of enhancing national and climate services (ENACTS), was used to visualize and analyze of the spatial characteristics of trends. The values of the formulas discussed in section 3.4.2.1 and section 3.4.2.2 were spatially visualized in maps to show the spatial characteristics.

3.4.3 Determination of the Spatial Characteristics of Current Flood Susceptibility the Study Region

To generate flood susceptibility maps, identifying the baseline factors that influence the flood occurrence for the study domain was the first step (Kamaraj & Rangarajan, 2022; Umaru & Adedokun, 2020). Therefore, the study identified 10 important factors that influence the region's flooding scenarios (shown in chapter 2 section 2.2). In this study, these factors were referred to as conditioning/baseline factors.

3.4.3.1 Description and Preparation of flood conditioning factors

3.4.3.1.1 Topographic Wetness Index

The topographic wetness index (TWI) represents the steady-state wetness index (Rocha et al., 2020). This index was used to compute the topographic control on the hydrological process and terrain driven variation in soil moisture (Rocha et al., 2020). This factor was calculated from the DEM with the raster calculator in Arc GIS using equation 6.0 (Costache, 2020).

$$\text{TWI} = \ln\frac{\propto}{\text{Tan}\,\beta} \tag{6.0}$$

Where $\propto$ denotes the local slope area drainage through a certain point x permeant contour length and β is the local slope in radians.

3.4.3.1.2 Slope and Elevation

This is calculated from the DEM of the Elgon region using the raster calculator in Arc GIS 10.5.The equation used based on the concept of the rate of change of elevation (dZ/dY) of elevation from one cell to another and the lateral directions (dZ/dX) from the central cell (Ro, 2001) as given in equation 7.0.

$$\text{Slope (degrees)} = \text{Arc Tan}\left(\sqrt{\left(\frac{dZ}{dX}\right)^2 + \left(\frac{dZ}{dY}\right)^2}\right) \tag{7.0}$$

Where dZ is denotes the difference in elevation between cells and dX and dY represent the horizontal distances between the central cell and its neighboring cell in the X and Y directions, respectively.

Higher elevation translated to lower probability to flood and lower elevation translated to higher likelihood to flood (Ogania et al., 2019; Rocha et al., 2020). This factor was derived from the DEM data of the Elgon region using Arc GIS 10.5.

3.4.3.1.3 Drainage Density

This factor represents the ratio of the cumulative distance of streams and rivers to the overall study domain area. High drainage density indicated low probability to flood and low drainage density indicated high probability to flood (Tariq et al., 2022). It was calculated from the Digital Elevation

Model (DEM) utilizing the raster calculator in Arc GIS 10.5 and classified. The drainage density was derived using a methodology proposed by (Hosseinzadeh, 2011) based on equation 8.0:

$$\text{Drainage density} = \frac{\sum_1^n L}{F} \quad (8.0)$$

where, l denotes the distance of the streams and rivers, n represents the number of streams and rivers and F represents the contributing drainage area.

3.4.3.1.4 Distance from the River

The distance from the river helps to define flood-prone areas along the river(Rahman et al., 2021). The Euclidean distance tool in ArcGIS was applied to calculate the approximate distance in meters of village centroids to the river. The tool was used to calculate the straight-line distance between points using equation 9.0.

$$\text{Euclidean Distance} = \sqrt{(x_2 - x_1)^2 + (y_2 - y_1)^2} \quad (9.0)$$

Where $(x_1\ ,\ y_1)$ represents the coordinates of the river point and $(x_2\ ,\ y_2)$ represent the coordinates of the centroid point.

3.4.3.1.5 Distance from the Road

Roads increase the speed and volume of surface runoff during heavy rainfall events (Tariq et al., 2022). The ArcGIS Euclidean distance tool was utilized to compute the approximate distance in meters from the road network to the Cell centroids. For each centroid, the Euclidian distance was calculated using equation 10.0.

$$\text{Euclidean Distance} = \sqrt{(x_2 - x_1)^2 + (y_2 - y_1)^2} \quad (10.0)$$

where $(x_1\ ,\ y_1)$ represent the coordinates of the road network point, and $(x_2\ ,\ y_2)$ represent the coordinates of the centroid point.

3.4.3.1.6 Rainfall

For this study, the rainfall data from CHIRPS spanning the years 1991 to 2022 was utilized. The study employed Climate data tools (CDT) to compute the annual climatology in terms of total average rainfall received using equation 11.0 and the result imported to ArcGIS 10.5.

$$Q = \frac{\sum_1^n R}{n} \tag{11.0}$$

Where R is the observed rainfall, Q denoted the annual average rainfall and n is the number of years.

3.4.3.1.7 Land Use Land Cover

The LULC map was classified into 12 classes, including built-up area, bushland, bulrospermum savanna, dry combretum savanna, farmland, forest/savanna mosaics, grass savanna, high alt forest, high alt moor and heath, moist combretum savanna, and seasonal wetland.

An unsupervised image classification was performed using the K-means clustering method. This method entailed clustering data into a predefined number of clusters (K) (Basheer et al., 2022). We began by strategically placing K centroids, one for each cluster, ideally far apart to ensure distinct results. Data points were then assigned to the nearest centroid, iteratively creating early groupings until all points were assigned (Basheer et al., 2022). Subsequently, new centroids were computed as the barycenter of their respective clusters, and this process was repeated until centroids no longer moved significantly. Finally, the algorithm seeks to minimize an objective function, specifically a squared error function represented by equation 12.0

$$\mathrm{J} = \sum_{\mathrm{j}=1}^{k} \sum_{\mathrm{i}=1}^{\mathrm{n}} (x_i - c_j)^2 \tag{12.0}$$

Where $(x_i - c_j)^2$ denotes a chosen distance measure between a data point x_i and the cluster center c_j denotes an indicator of the distance of n data points from their respective cluster centers.

3.4.3.1.8 Normalized Difference Vegetation Index

NDVI was computed using equation 13.0 as the ratio of the Red band reflectance value of a pixel (B4) and the near-infrared band reflectance value of a pixel (B5) bands of satellite imagery.

$$\text{NDVI} = \left(\frac{B5-B4}{B5+B4}\right) \quad (13.0)$$

High positive NDVI values symbolize lush and healthy vegetation, whereas low or negative NDVI values suggest limited or no vegetation presence.

3.4.3.1.9 Soil Types

Data information about soil types in the study that was used for reclassification was acquired from the Food and Agriculture Organization (FAO) website (https://www.fao.org/soils-portal/data-hub/soil-classification/en/).

The reclassification process to categorize various soil types based on their inherent characteristics. This classification aimed to group similar soil types together, considering factors such as texture, drainage properties, and permeability

3.4.3.2 Analytical Hierarchy Process

The conditioning factors discussed in section 3.3.2.1 were ranked using the Analytical Hierarchy Process (AHP) methodology to identify the individual level of influence in terms of impact weight to the floods (Findayani et al., 2019). AHP tool, developed by (Saaty, 1987), aided the decision making and evaluation and prioritization of multiple factors affecting flood susceptibility by structuring the individual factors, performing pair-wise comparisons to define significance expressed as a matrix in scale of 1-9 to represent neutral all through to extreme importance(Table 3) and calculating weights using the random Index (RI) of consistency to ensure consistency of the pair-wise comparisons.

Table 3: AHP pairwise comparison rating fundamental scale (Saaty, 1987)

Degree of significance	Definition	Explanation
1	Equal significance	The two factors have the same importance
3	Moderate significance of one over another	One factor is moderately superior to another based on experience and judgment.
5	Strong significance	One factor is essentially or strongly superior to another based on experience and judgment
7	Very strong significance	One factor is very strongly superior to another based on experience and judgment. And its power is reflected in practice.
9	Extremely significant	One factor is extremely superior to another based on experience and judgment. And its power is reflected in practice. The evidence for the effectiveness of one criterion over another is of the greatest degree of confirmation
2,4,6 and 8	Intermediately significance between two above adjacent preferences	Used to indicate the compromises between the two above judgments or significance 1,3,5,7, and

The Consistency Ratio (CR) was identified as a ratio of consistency index (CI) to random consistency Index as shown in equation (14.0) whereas CI was calculated using equation (15.0).

$$\mathrm{CR} = \frac{\mathrm{CI}}{\mathrm{RI}} \tag{14.0}$$

$$\mathrm{CI} = \frac{\lambda_{\mathrm{max-n}}}{\mathrm{n-1}} \tag{15.0}$$

Fundamental components in calculating CR were the average of the consistency vector, represented by λ, RI which denotes the Random Consistency index, and CI is the consistency index.

The final value of the CR of less than 0.1 was considered to validate the weights. Once the pairwise comparison and consistency was ensured, weights were calculated for each factor reflecting its relative importance in contributing to flood susceptibility.

3.4.3.3 Weighted overlay

ArcGIS weighted overlay tool was used to combine multiple spatial datasets into a single layer using equation 16.0 (Tariq et al., 2022). This technique takes into account the relative importance of each conditioning factor obtained in section 3.3.2.1.2 and the reclassification according to the susceptibility class rating.

$$\text{Weighted overlay} = \sum_{i=1}^{n}(f_i . W_i) \quad (16.0)$$

Where i signifies the index representing individual flood conditioning factors ranging from 1 to n, each factor is denoted as f_i corresponding to a specific value associated with a particular cell and finally W_i represents the weight assigned to the ith factor , reflecting its relevant importance.

Equation 16.0 was applied to compute the weighted overlay value for each cell. Following the computation of the weighted overlay, the generated raster file delineated areas of varying flood prone areas in square kilometers with response units of very low, low, moderate and high to very high there by generating a susceptibility map. This method was also used in studies by (Edamo et al., 2022; Tariq et al., 2022).

3.4.4 Prediction and Mapping of Future Flood Susceptible Areas of the Study Region

Additional adjustments and modifications on the methodology described in section 3.4.4 were made to address the projected flood prone areas under a climate change. To achieve this, the rainfall projections were used to examine the possible influences of such alterations to floods along with the conditional factors, including TWI, slope, elevation, distance from the road and river, soil type, drainage system, and NDVI discussed in section 3.4.3.1 – 3.4.3.8.

The conditioning factors were reclassified and ranked with the AHP tool discussed in section 3.4.3.9 to determine the individual level of influence in terms of impact weight to the floods (Findayani et al., 2019). The consistency ratio (CR) was computed using equation 14.0 and equation 15.0 above.

ArcGIS weighted overlay tool was used to combine multiple spatial datasets into a single layer using equation 17.0 (Tariq et al., 2022),

$$\text{Weighted overlay} = \sum_{i=1}^{n}(f_i \; X \;\; W_i) \qquad (17.0)$$

Where i signifies the index representing individual flood conditioning factors ranging from 1 to n, each factor is denoted as f_i corresponding to a specific value associated with a particular cell and finally W_i represents the weight assigned to the ith factor, reflecting its relevant importance.

This technique takes into account the relative importance of each conditioning factor obtained in section 3.4.3.10 and the reclassification according to the susceptibility class rating.

Equation 17.0 above is used to calculate the weighted overlay value for each cell. Following the computation of the weighted overlay, the generated raster file delineated areas of varying flood prone areas in square kilometers with response units of very low, low, moderate and high to very high there by generating a susceptibility map. This method was also used in studies by (Edamo et al., 2022; Tariq et al., 2022).

3.4.5 Determination of the Impacts of the Projected Floods on Farmland Food Security

3.4.5.1 Farmland Mapping

Farmland mapping was performed by using base data of LULC of the same study domain and the digitizing tool provided in ArcGIS software version 10.5. This was executed using polygon digitization where the farmlands were outlined and extracted from the Land Use Land Cover map (Kamaraj & Rangarajan, 2022). This approach aligns with the methodology employed by (Chau et al., 2013; Dede et al., 2022). Dede et al., (2022) used the methodology to determine the changes in the agricultural sites while (Chau et al., 2013) used the same method to map impacts of extreme floods on agriculture.

3.4.5.2 Mapping the Impact of flooding to Agriculture

The digitized farmlands map was used to identify agricultural land areas prone to flooding (Muhammad et al., 2022). The farmland data was overlaid with the flood hazard data for each RCP scenario. The digitized farmland area was subjected to an intersection analysis with the flood of the different Representative Concertation Pathways (RCPs) in section 3.4.4.

The intersect analysis computes the geometric overlap between multiple feature classes and layers. It identifies and retains the features or segments of features that are shared by all input sources. These common areas of overlap are then recorded in the resulting output feature class, highlighting only the regions where the input sources intersect to GIS-based Flood Susceptibility.

Finally, the flood prone farmlands were constructed for the period 2030-2050 for the RCPs 2.6, RCP4.5, and RCP 8.5 and areas that ranged from low to very high were mapped. OPM, (2020) and Roopnarine et al., (2018) adopted a similar approach to perform a GIS based Risk mapping.

CHAPTER FOUR

RESULTS AND DISCUSION

4.1 Introduction

This chapter presents the results and discussion based on the methods used to analyze the specific objectives of the study.

4.2 Homogeneity test

Figure 3 presents plots of cumulative annual rainfall for Bududa, Kapchorwa and Mbale against time for the period 1991-2022.

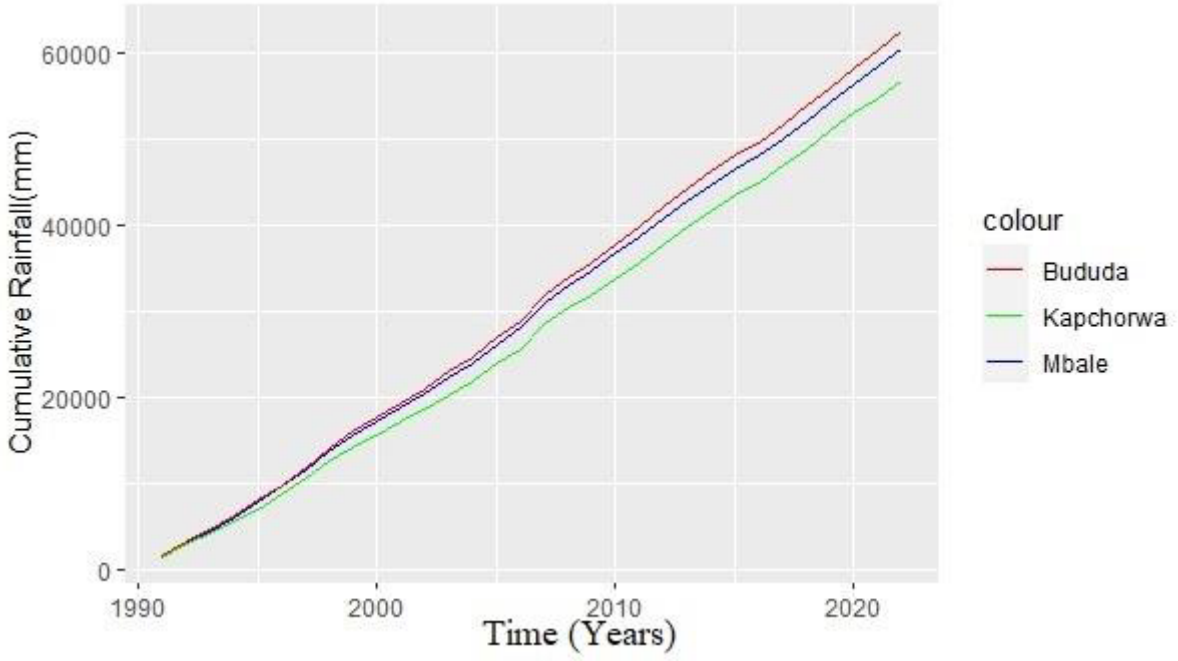

.

Figure 3: Cumulative plots of annual rainfall (mm) for the year 1991 - 2022 in three representative observation points (Bududa, Kapchorwa and Male) illustrating homogeneity test.

The straight line in the cumulative annual rainfall plots for the three regions (Bududa, Kapchorwa, and Mbale) indicates homogeneity in the used data and confirmed that the data was fit for use.

4.3 Seasonal Precipitation Patterns

The trends of observed rainfall data for the season of March, April, May (MAM), September, October, November (SON), June, July, August (JJA) and December, January, February (DJF) were analyzed using R software version 4.3.2 for all the six observation points and are presented and discussed in the following sub-sections.

4.3.1 Temporal characteristics of Rainfall in MAM Season

Table 4 presents the results of the rainfall analysis for the MAM season, unveiling diverse patterns across the study area. Figure 4 illustrates the trends at the six observation points, with Mbale, Bududa, Bunginyanya, and Sironko displaying an increasing trend, supported by positive S and Z values in table 4 and a rising trend line (blue) in Figure 4. Despite the upward trajectory, statistical significance was lacking during the MAM season, as indicated by a P-value exceeding the 0.05 significance level in table 3. Moreover, the Sen's slope estimator, at a 95 percent confidence interval, reported increases of magnitude 2.616, 2.886, 3.165, and 3.405 for Mbale, Bududa, Bunginyanya, and Sironko, respectively.

Table 4: Trends in MAM season (1991-2022) at various observation points in the Elgon region.

	Mann-Kendall trend test				**Sen's slope**	
	Z	P-VALUE	S	VARS	slope	
Mbale	1.4757	0.06	92	3802.6	2.615669	positive
Bududa	1.7027	0.076	106	3802.6	2.8858	positive
Kapchorwa	2.1244	0.033	132	3802.6	4.4947	positive
Bunginyanya	1.2162	0.06	76	3802.6	3.165	positive
Bukwo	2.1568	0.031	134	3802.6	4.2807	positive
Sironko	1.8649	0.0622	116	3802.6	3.4058	positive

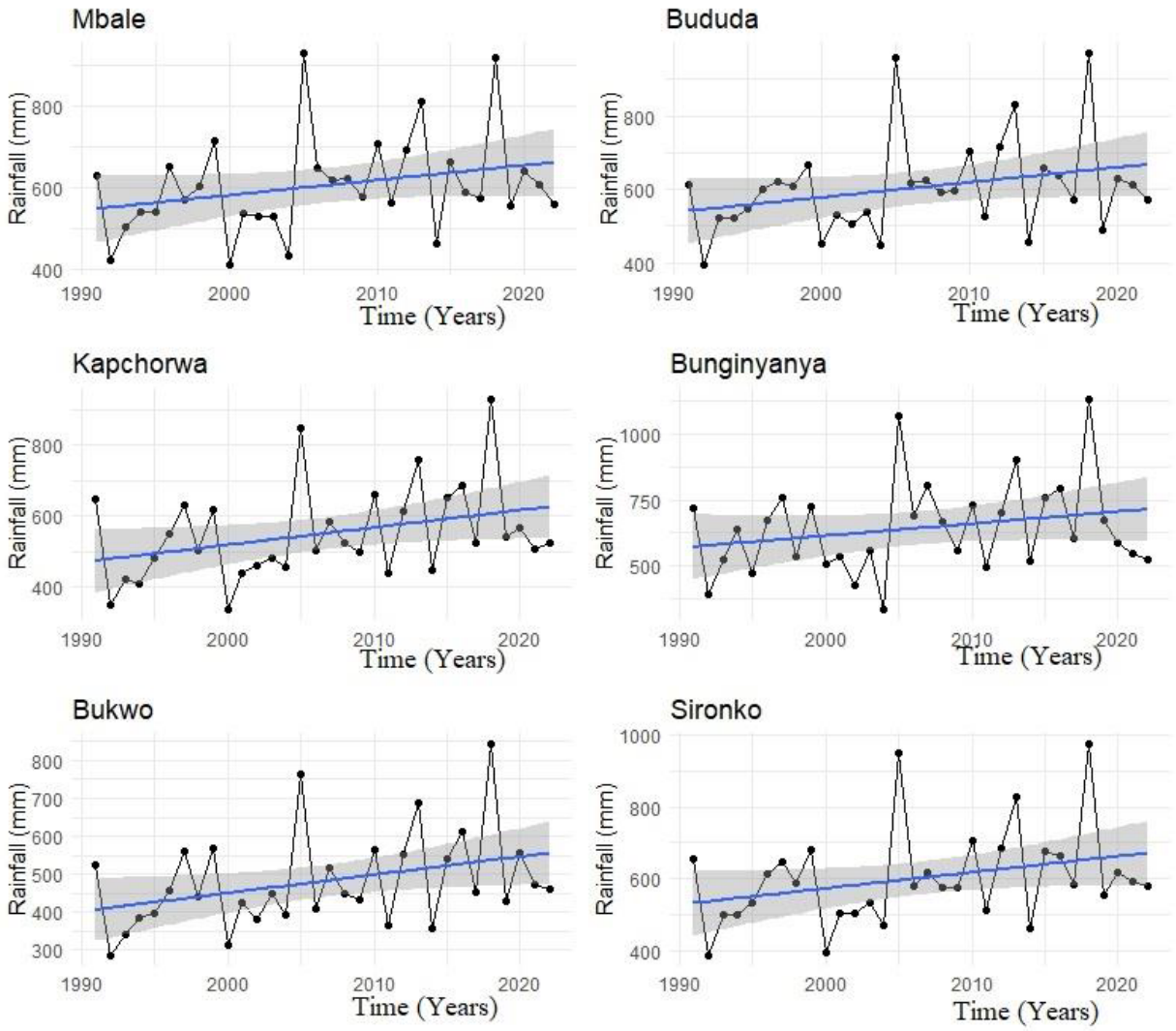

Figure 4: Time series of MAM Seasonal rainfall from 1991 - 2022 represented by Mbale, Bududa, kapchorwa, Bunginyanya, Bukwo and Sironko. The solid blue line indicates the trend line.

On the other hand, Kapchorwa and Bukwo observation points showed an upward significant increasing pattern in the overall rainfall was detected during MAM season as the P-value associated with these areas were below the significance level of 0.05 (0.033 and 0.031) respectively and positive S and Z values as shown in Table 4 as well as the trend line in Figure 4.

Furthermore, the positive values of the Sen's slope estimator signify an increasing trend of magnitude range 4.4947 and 4.2807 (Table 4) at a 95 percent confidence.

Overall, the MAM season rainfall analysis showed that the rainfall received in the region was increasing as shown by the increasing trend and these findings highlight the heightened degree to

which the area is prone to flooding especially areas in Bukwo and Kapchorwa where the increase is significant.

4.3.2 Temporal characteristics of Rainfall in SON Season

Unlike the MAM season, the trend test conducted over the SON season indicated a statistically significant trend in all the six observation points, with P-values less than 0.05 significant level (Figure 5 and Table 5). This trend was increasing as shown by the S and Z values shown in table 5. More to that, at the 95 percent interval, the positive values of the Sen's slope, as illustrated in table 5, suggested an increasing trend of magnitude that ranged between 5.90527 and 10.30357 in rainfall over time during the SON season also shown by the steep slope of the trend line in Figure 5 indicating the strength and consistency of the increasing trend.

Table 5: Trends in SON season (1991-2022) at various observation points in the Elgon region.

	Mann-Kendall trend test				**Sen's slope**	
	Z	P-VALUE	S	VARS	slope	
Mbale	2.7406	0.022	179	3802	5.90527	positive
Bududa	2.6108	0.041	162	3802	7.61479	positive
Kapchorwa	3.2271	0.024	200	3802	8.343801	positive
Bunginyanya	2.546	0.004	158	3802	10.30357	positive
Bukwo	3.0649	0.051	190	3802	7.561117	positive
Sironko	2.8054	0.034	174	3802	8.207982	positive

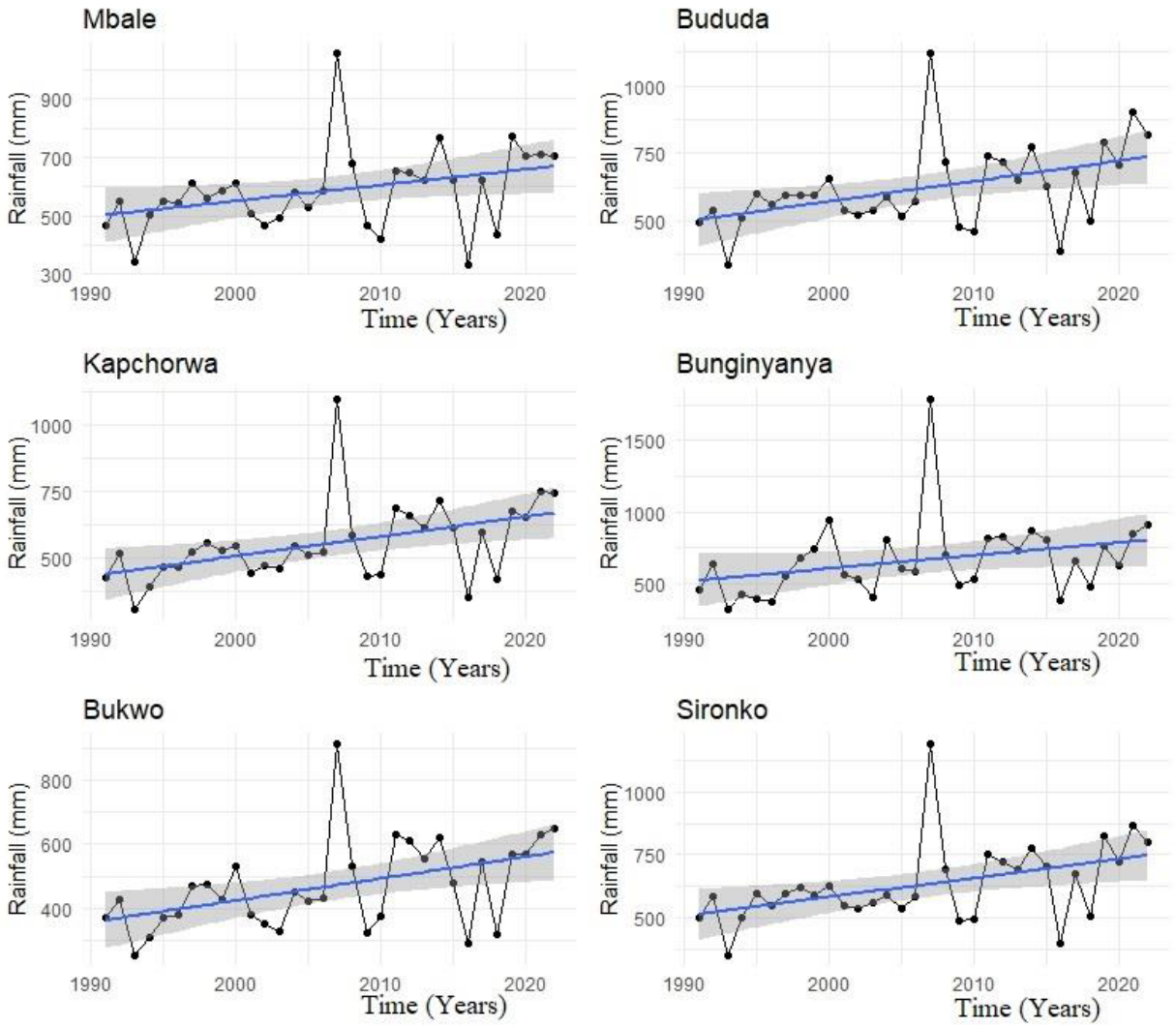

Figure 5: Time series of SON Seasonal rainfall from 1991 - 2022 in the study area represented by Mbale, Bududa, Kapchorwa, Bunginyanya, Bukwo and Sironko. The solid blue line indicates the trend line.

SON season is characterized as the short rainy season of the region and these findings signify a potential intensification of the second rainy season in the Mount Elgon region (McKinney & Wright, 2021). As shown in Figure 5, the increase in rainfall observed during SON has resulted in higher total amounts of precipitation over the years as observed that 2001 registered the peak rainfall, while 2016 witnessed the lest total rainfall across of observation points. The trend line indicates steep slopes hence affirming a significant increasing trend in the SON season.

The study of rainfall trends in the SON season identified the intensification of the short rainy season that may likely increase the area prone to flooding and consequently disrupt agricultural activities and food security.

4.3.3 Temporal characteristics of Rainfall in JJA Season

The analysis of trends in the JJA season, presented in Figure 6 and Table 6, reveals an increasing pattern indicated by the S and Z values. However, the trend is not statistically significant at the 0.05 significance level for all six observation points in the region. The P values for Male, Bududa, Kapchorwa, Bunginyanya, Bukwo and Sironko range from 0.1084 to 0.3140 as shown in Table 6 were all greater than 0.05 significance level. This implies that there is no definitive evidence of the significant trend in the rainfall during those specific seasons in the study area. However, at a 95 percent interval, the positive values of the magnitude of the Sen's slope estimator which ranged from 2.9625 to 4.271 (Table 6).

Table 6: Trends in JJA season (1991-2022) at various observation points in the Elgon region.

	Mann-Kendall trend test				**Sen's slope**	
	Z	P-VALUE	S	VARS	slope	
Mbale	1.346	0.1783	84	3802	3.259796	positive
Bududa	1.2162	0.2239	78	3802	2.962476	positive
Kapchorwa	1.8	0.2719	112	3802	4.270972	positive
Bunginyanya	1.2811	0.2002	80	3802	4.14875	positive
Bukwo	1.4757	0.3140	92	3802	3.904036	positive
Sironko	1.6054	0.1084	100	3802	4.069317	positive

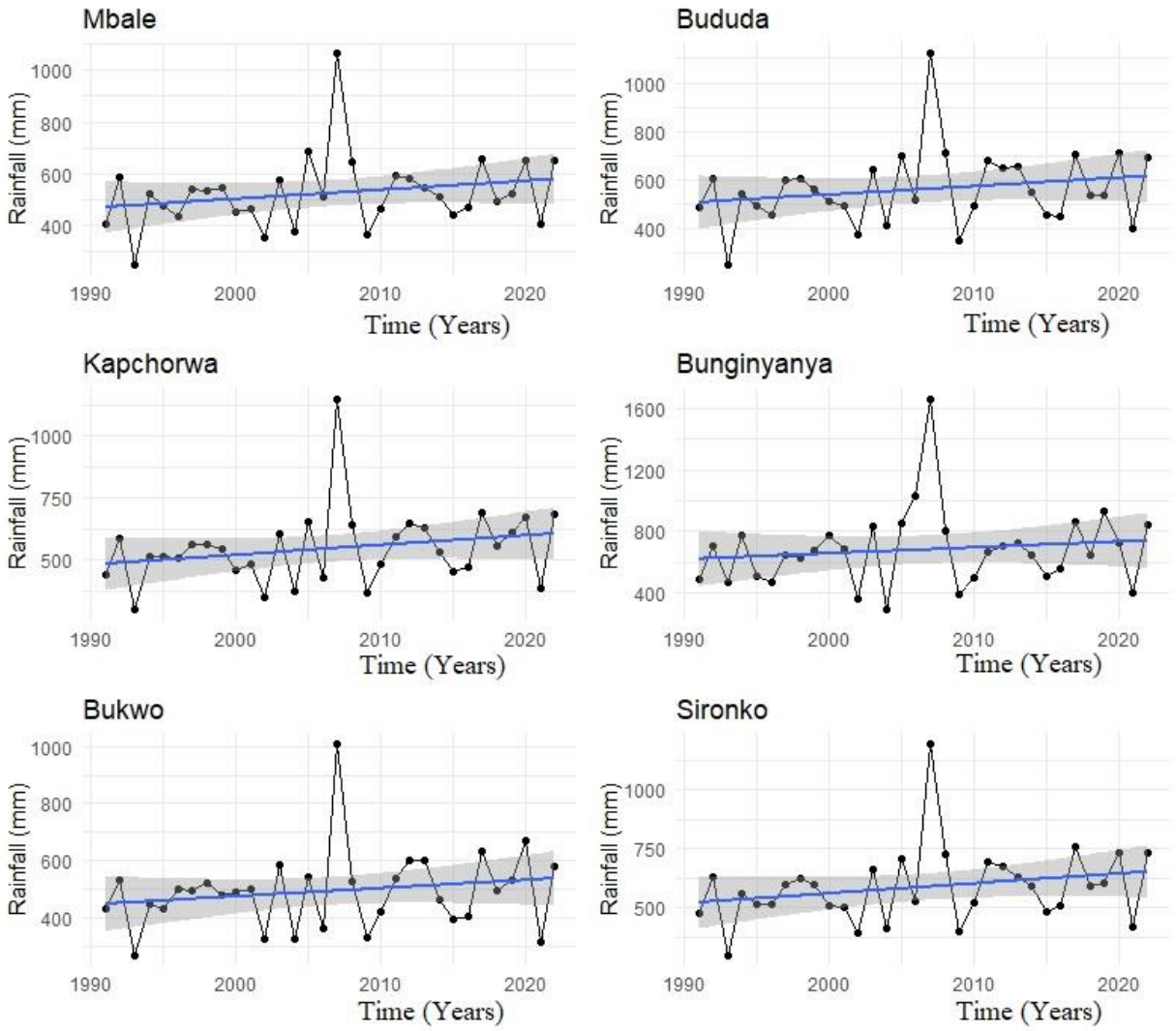

Figure 6: Time series of JJA Seasonal rainfall from 1991 - 2022 in the study area represented by Mbale, Bududa, Kapchorwa, Bunginyanya, Bukwo and Sironko. The solid blue line indicates the trend line.

The total seasonal rainfall observed in all the six points for a period of 1991 – 2021 is less than 800mm with exception of year 2007 where the total rainfall exceeded 1000mm across the area.

Although statistical significance was absent in the observed trends during the JJA season, it is worth noting that the analysis revealed an increasing pattern in the total rainfall received over the years. This suggests that there is a significant positive trend of rainfall that may contribute to changes in the flood prone areas.

4.3.4 Temporal characteristics of Rainfall in DJF Season

In the DJF season as shown in figure 7 and table 7, the rainfall trend was upward and increasing as shown by the S and Z values shown in table 7. Mbale, Bududa, and Sironko exhibited P-values greater than 0.05 significance level (0.423, 0.321, and 0.4655) respectively, indicating non-significant trends in these areas. Similarly, Kapchorwa and Bukwo exhibited non-significant pattern as P-values of 0.543 and 1.408, respectively at 0.05 significance level were detected. Bunginyanya demonstrated the highest P-value of 0.567 among all observation points, further reinforcing the non-significant trends in rainfall during the DJF.

Notably, the positive slopes for all observation points (ranging from 0.4621 to 1.6182) shown in Table 7 indicate an increasing pattern in rainfall of varying magnitude over the DJF season. Although not statistically significant, this rising trend suggests a tendency towards higher precipitation amounts during the winter months in the region

Table 7: Trends in DJF season (1991-2022) at various observation points in the Elgon region.

	Mann-Kendall trend test				**Sen's slope**	
	Z	P-VALUE	S	VARS	slope	
Mbale	0.82704	0.423	52	3802	0.8218333	Positive
Bududa	0.69731	0.321	44	3802	0.5425425	positive
Kapchorwa	1.0541	0.543	66	3802	1.174981	positive
Bunginyanya	1.4759	0.567	92	3802	1.61825	positive
Bukwo	0.82704	1.408	52	3802	0.4621477	Positive
Sironko	0.72974	0.4655	46	3802	0.8245107	positive

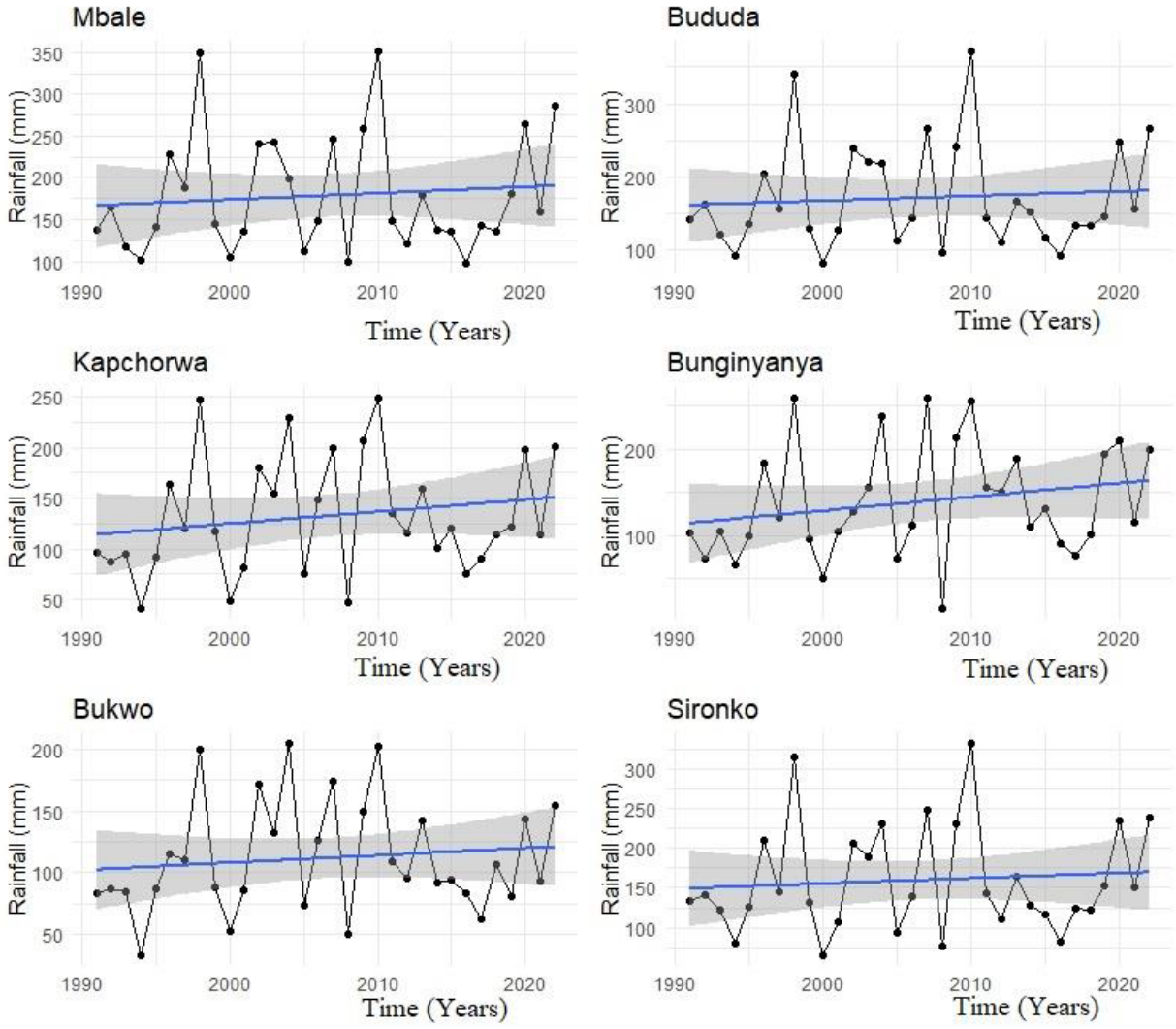

Figure 7: Time series of DJF Seasonal rainfall from 1991 - 2022 in the study area represented by Mbale, Bududa, Kapchorwa, Bunginyanya, Bukwo and Sironko. The solid blue line indicates the trend line.

4.3.5 Spatial Distribution of Seasonal Rainfall Trends

Figure 8 presents the distribution of rainfall trends in the Mount Elgon region of Uganda over the period 1991 – 2022.

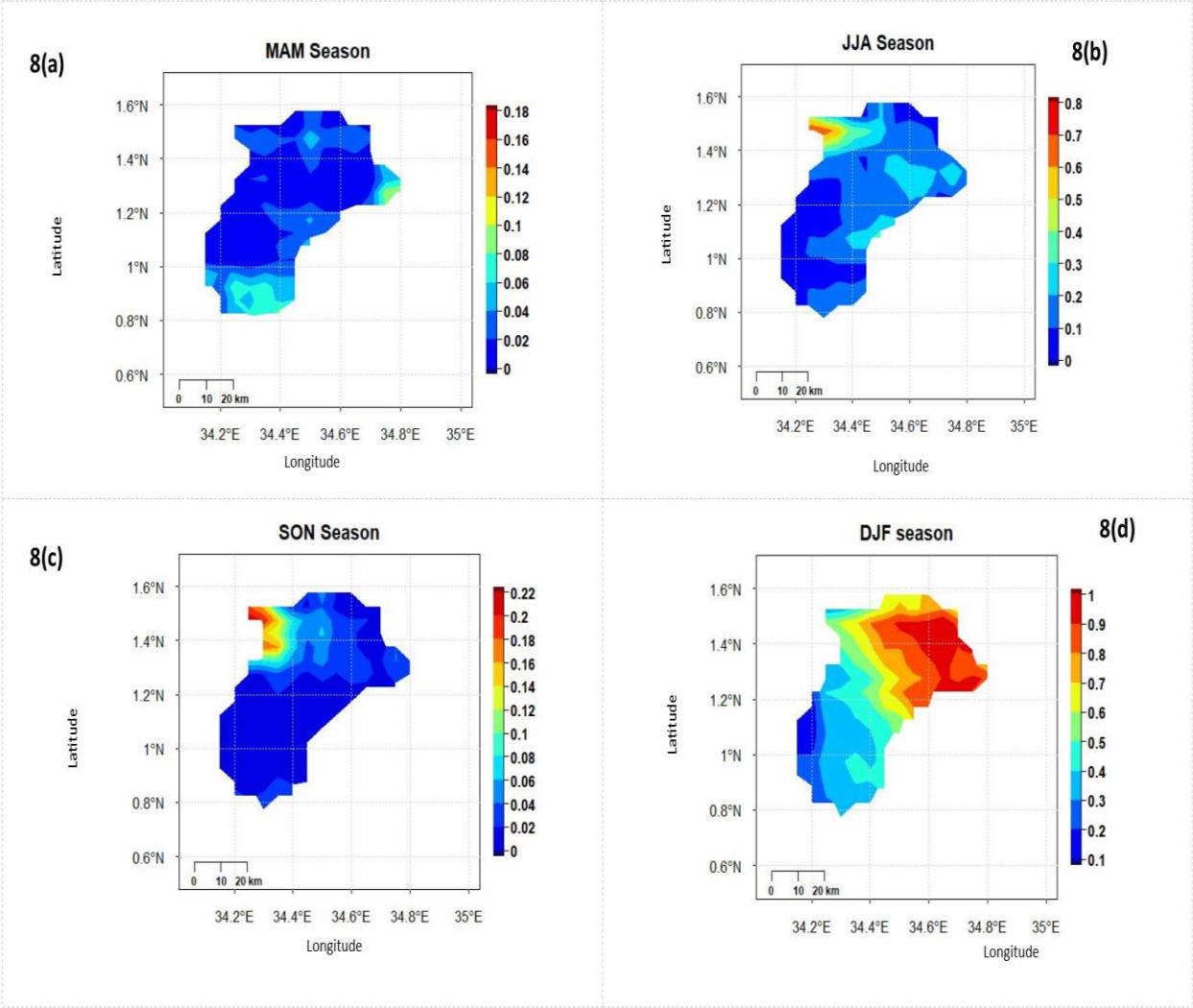

Figure 8: Spatial distribution of trends in Rainfall over the period of 1991-2022, the legend describes P-values at a 0.05 significance level.

During MAM season, figure 8 (a), non-significant trends with values of greater than 0.05 significance level were detected in the south and north parts of the region. However, the rest of the region exhibited significant trends, indicating notable changes in the rainfall patterns during this season as values were greater than 0.05 significance level.

In JJA season, figure 8 (b), the seasonal rainfall distribution has a variable pattern with high rainfall mostly distributed in the northern part and decreases as you move to the south. In SON season, figure 8(c) however, the spatial plots indicated consistent patterns of rainfall as the whole region experienced significant trends. In DJF season figure 8 (d), non-significant trends were observed throughout the entire region. However, higher values of the rainfall trends were noted in the North

and North-East areas compared to the central and the southern areas hence spatial gradient in rainfall patterns during the DJF season**.**

The observed spatial distribution of seasonal rainfall trends highlights the heterogeneity within the Elgon region. Different seasons exhibit varying patterns of rainfall trends, with notable spatial variations across the region.

The study results are consistent with those reported by (Kansiime et al., 2013), emphasizing the diverse rainfall trends within the Elgon region. Various seasons display distinct patterns of significance and non-significance.

Areas experiencing significant trends in rainfall may be more prone to floods, with negative implications for food security. Finally, the presence of significant trends in certain seasons suggests that these seasons may be associated with the increased flood risks in the region of study.

4.4 Spatial Characteristics of Current Flood Susceptibility

To map the spatial characteristics of current flood susceptibility in ArcGIS, the study employed a set of ten conditioning factors as discussed below (Costache, 2020; Edamo et al., 2022; Tariq et al., 2022).

4.4.1 Flood Conditioning Factors

As presented in chapter two section 2.3, the flood susceptibility in this study was mapped using 10 conditioning factors to include; topographic Wetness Index, elevation, slope, rainfall, land use land cover, Normalized Difference vegetation index, distance from the river and road, drainage density and soil type. All these factors were collected from various sources projected to WGS 1984 projected coordinate system in ArcGIS 10.5 as discussed below.

4.4.1.1 Topographic Wetness Index

The calculated TWI from Equation 6.0 values were spatially represented across the study area with values that ranged from -21.3 to 12.5 as shown in Figure 9. The TWI was clustered into five classes ((-21.3) – (-17.0)), ((-17.1) – (-13.8)), ((-13.9) – (-6.8)), ((-6.9) – (2.2)), (2.3 – 12.5) and classified as very low (1), low (2), moderate (3), high (4), very high (5) respectively. The Map depicts

variations in terrain wetness, with low values indicating well-drained areas with efficient water flow and the higher values indicate areas with higher potential for water accumulation (Rocha et al., 2020). This map indicates that low lying areas of the mount Elgon region is highly susceptible to flooding compared to the high slopes.

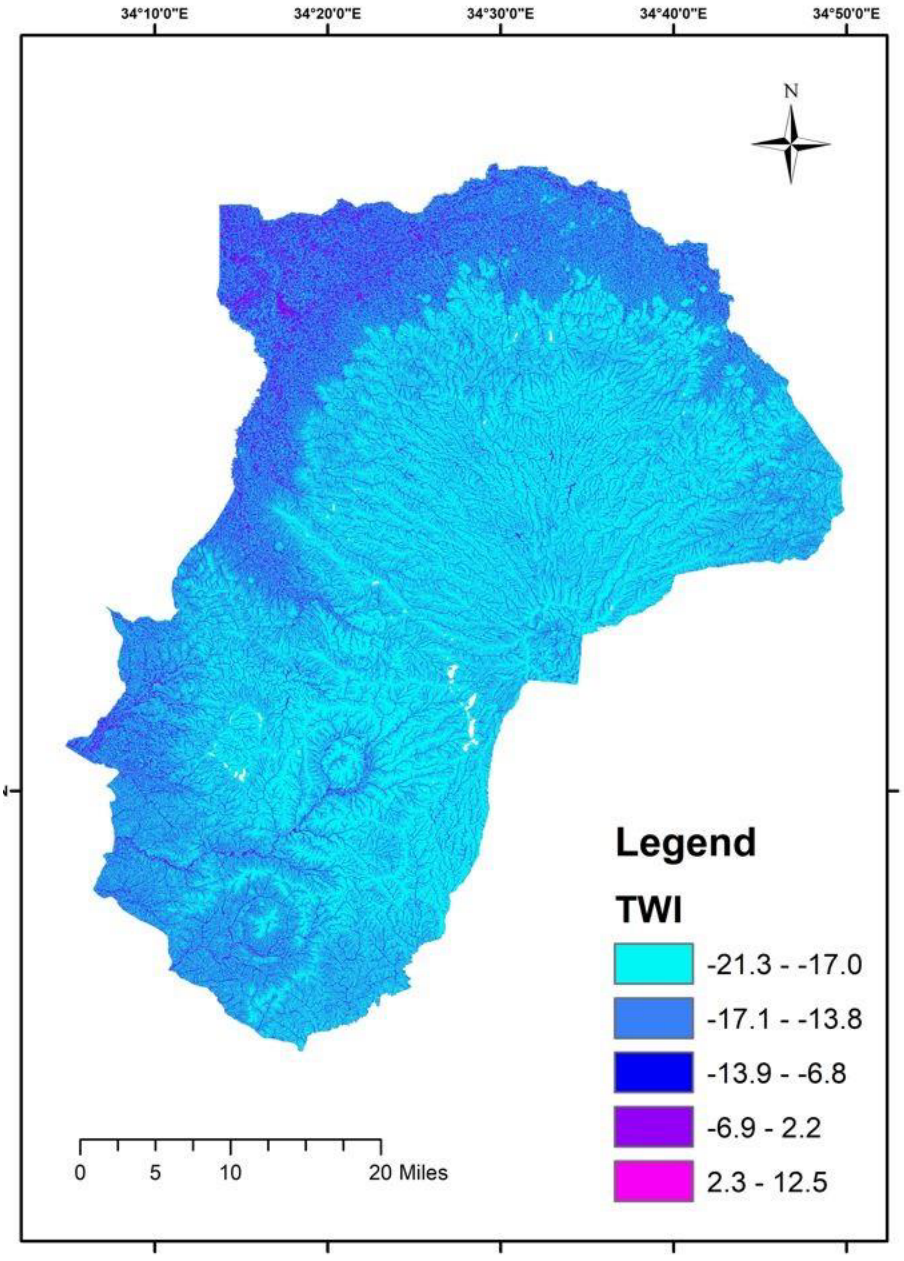

Figure 9: Map of Mount Elgon region showing Spatial distribution of TWI.

4.4.1.2 Elevation

Figure 10 revealed that the study area elevation ranged from 1044m to 4320m above sea level. It was classified into clases depending on the influence of terrain on flooding. Areas of low elevation (1,044 -1,326) were classified as very highly prone to flood followed by 1,37 -1,789 as high, 1790 – 2392 as moderate, 2,393-3,150 as low and high elevation areas of 3,151 -4320 as very low flood areas. This agrees with results that were presented by O'Donnell & Thorne, (2020) which indicated the low elevation at the downstream as areas prone to flooding and higher elevation in the upstream as areas of low flood susceptibility.

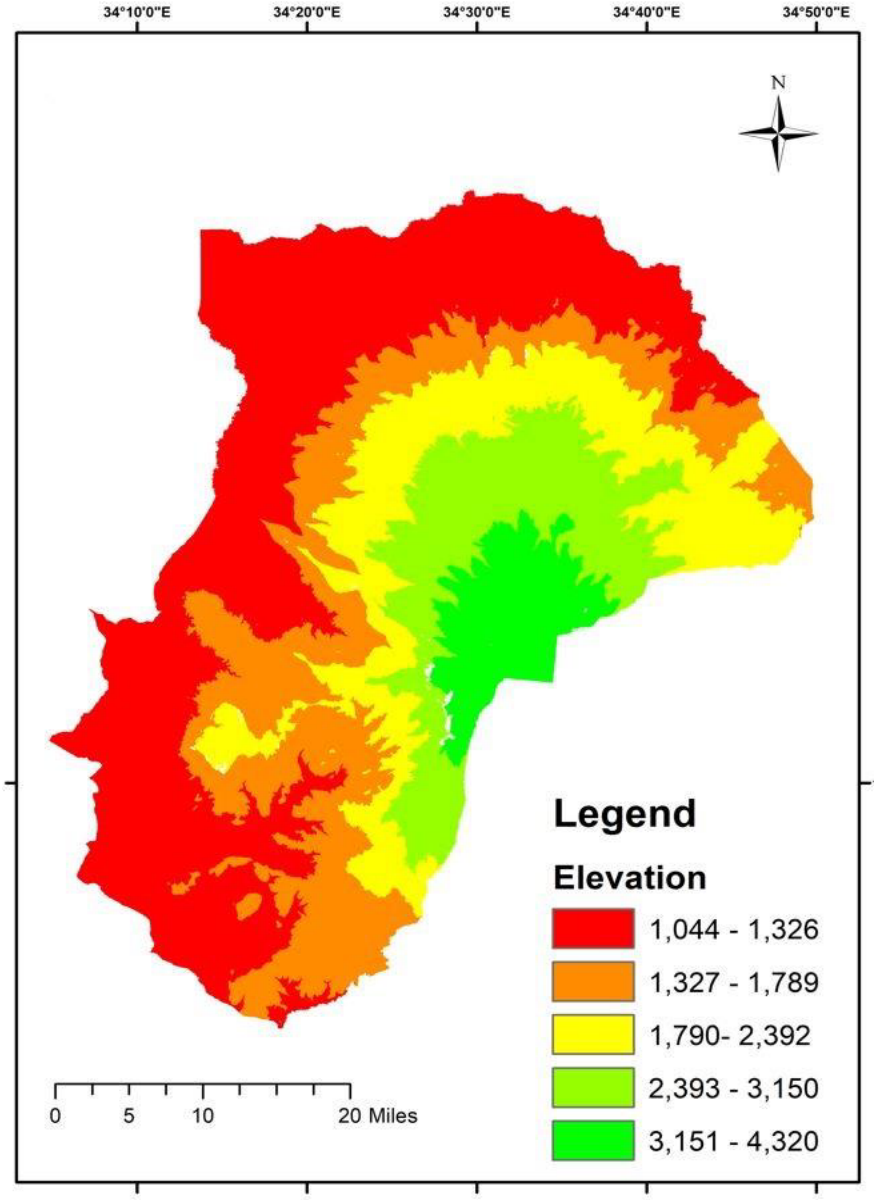

Figure 10: Map of Mount Elgon region showing Spatial distribution of Elevation (b)

4.4.1.3 Slope

The slope values in the mount Elgon region ranged from 0 to 54 degrees and fell into five classes of 0 – 6, 7-15, 16 – 26, 27 – 39 and 40 – 54, as very high (5), high (4), moderate (3), low (2), very low (1) respectively. It indicates that areas with lower slope values increase the risk of water accumulation have greater risk of the area being highly prone to flooding than areas with higher values of the slope. This aligns with the previous studies (Kamaraj & Rangarajan, 2022; Rocha et al., 2020; Tariq et al., 2022) whose findings correlate that lower slope are associated with flood susceptibility and high slope areas with low flood susceptibility.

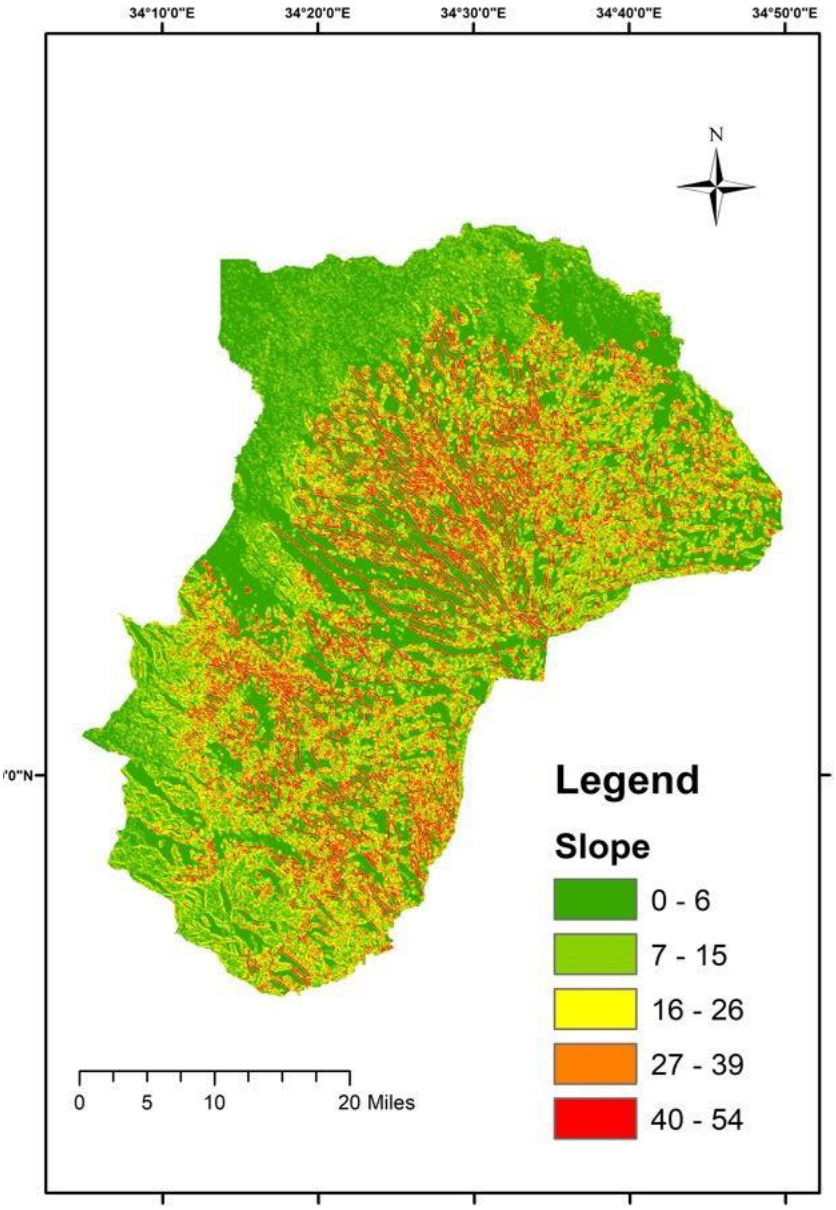

Figure 11: Map Mount Elgon region showing Spatial distribution of slope.

4.4.1.4 Drainage Density

The drainage density generated from the spatial analyst tool of "line density" analysis of flow accumulation represented by figure 12 ranged from 13 to 229 and was classified as (13 - 56), (57 – 99), (100 -142), (143 – 185), (185 – 229) and classified as very low (1), low (2), moderate (3), high (4) and very high (5) respectively. Areas with higher drainage density were in the low land of the region and are highly prone to flooding and area of low drainage density are in the highlands

of the region and less prone to flood and previous studies support this (Rocha et al., 2020; Tariq et al., 2022).

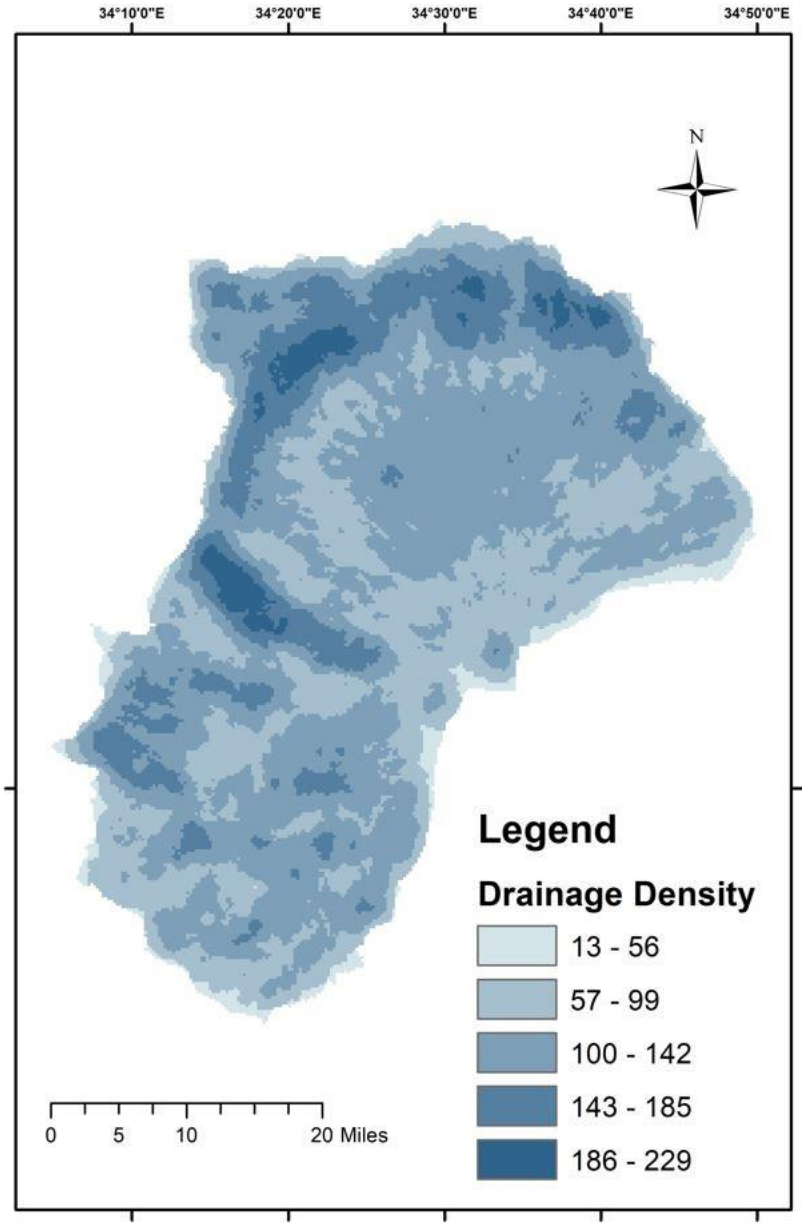

Figure 12: Map Mount Elgon region showing Spatial distribution of drainage density.

4.4.1.5 Distance from the River

Figure 13 considered areas between 0-3,302 meters are high flood prone areas as compared to other areas because its distance considers the river's floodplain width and the potential for lateral flow during extreme events. Areas at (3,303-6,605), (6,606-9907), (9,907-13,210), and (13,210-16,513) were classified as high, moderate, low, and very low respectively.

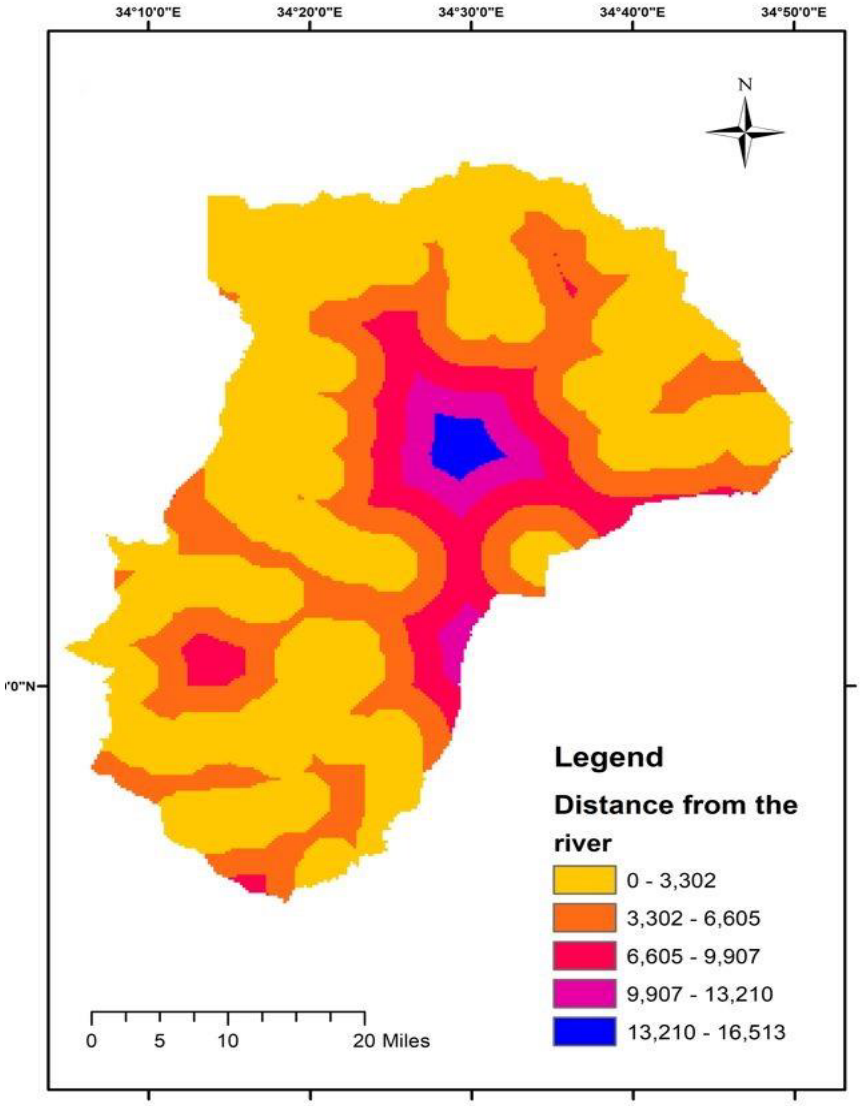

Figure 13: Map of Mount Elgon region showing Spatial distribution of distance from the river.

The interplay between proximity to the river and floodplain dynamics is a crucial factor. Scholars acknowledge that the flood-plain area extends to a distance that is directly influenced by the river's natural variability in water levels during flood events. This study identifies that in the Elgon region, floods are common in areas about 3km from the river. More to that, (Umaru & Adedokun, 2020) considered an distance above 3000 meters to be the more susceptible to flooding, especially during periods of heavy rainfall or river overflow.

4.4.1.6 Distance from the Road

As shown in figure 14, the study found that distance from the road had a small influence on the areas prone to flood in the region as compared to distance from the river. None the less, the study considered that areas located within 4,510 meters from the road were Very High flood-prone areas, areas situated between 4,510 - 9,021 meters from roads fell within the High flood-prone category, indicating a significant risk of flooding in these regions.

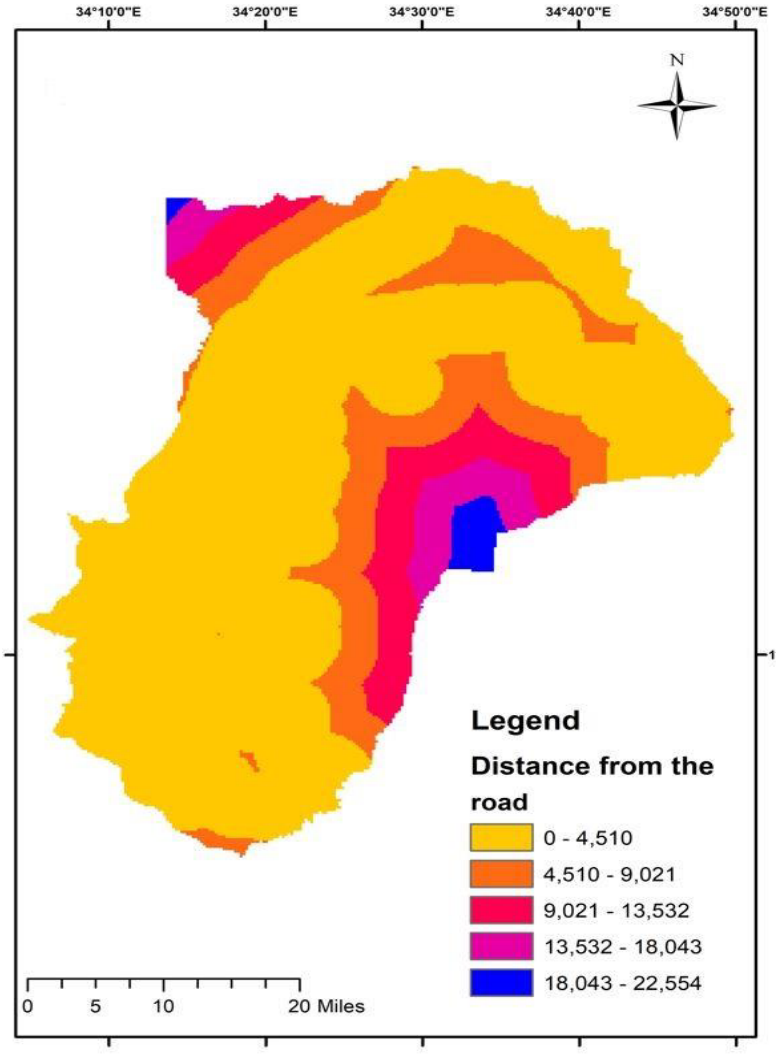

Figure 14: Map of Mount Elgon region showing Spatial distribution of distance from the road.

Moderate flood susceptibility was observed in areas located between 9,021 to 13,532 meters from roads, signifying the potential for flood-related challenges. Meanwhile, areas extending from 13,532 to 18,043 meters from roads are considered Low flood-prone regions, indicating a comparatively reduced flood risk. Areas positioned at a distance of 18,043 to 22,554 meters from

roads are characterized as Very Low flood-prone zones, suggesting a lower susceptibility to flooding.

4.4.1.7 Land Use Land Cover

LULC data was obtained from 2019 Landsat 8 OLI imagery from the USGS website. Figure 15 presents the different categories of the LULC of the Elgon region classified into 12 classes as built-up area, bushland, bulrospermum savanna, dry combretum savanna, farm land, forest/savvana mosaics, grass savanna, high alt forest, high alt moor and heath, moist combretum savanna and seasonal wetland.

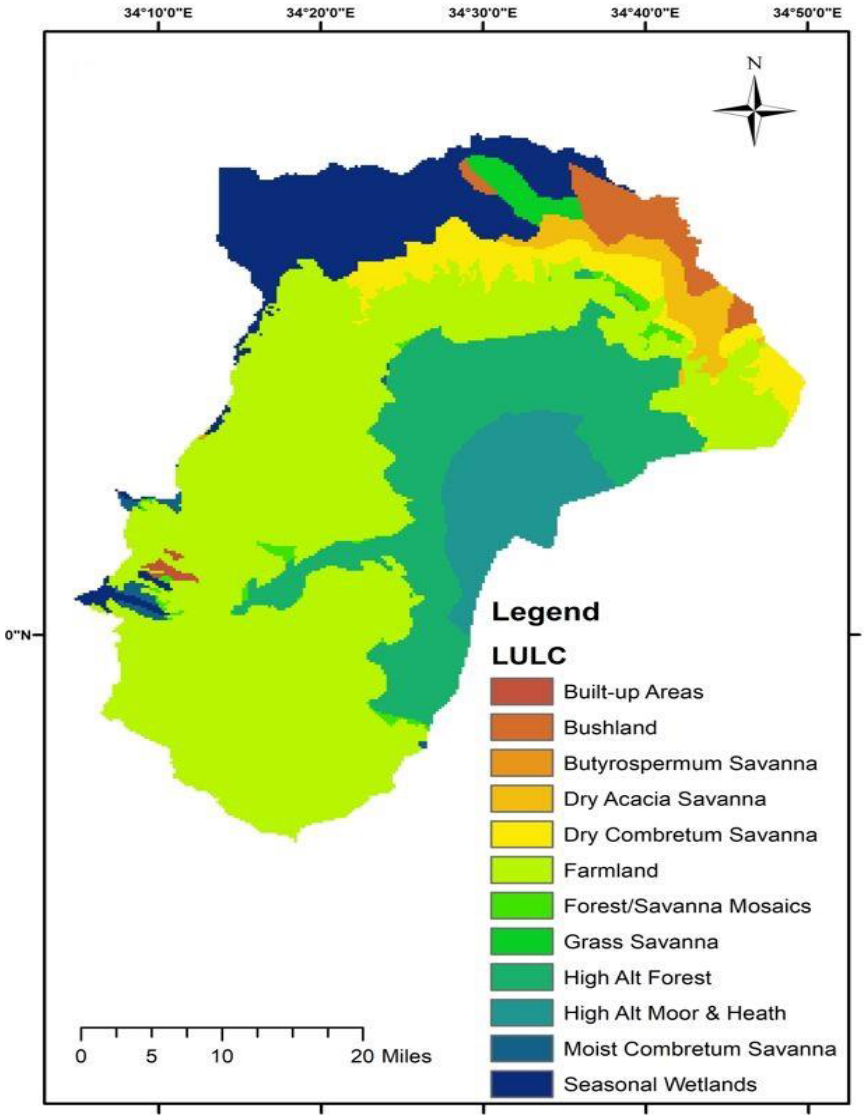

Figure 15: Map of Mount Elgon region showing Spatial distribution of LULC.

4.4.1.8 Normalized Difference Vegetation Index

The NDVI the ranged from -1.0 to 1.0 (Figure 16), signifying vegetation density and vitality. Negative values predominantly arise from elements such as clouds, water, and snow, while values close to zero primarily result from rock and exposed soil. Very low NDVI values (0.1 and below) correspond to areas devoid of vegetation, such as rocky, sandy, or snowy terrains. Moderate values (0.2 to 0.3) are characteristic of shrub and grassland regions, while high values (0.6 to 0.8) are indicative of temperate and tropical rainforests areas with low NDVI suggested that the area has limited vegetation making them more susceptible to flooding where as higher NDVI values indicate areas with denser and healthier vegetation cover, which are likely to be less flood-prone due to better water retention and reduced surface runoff.

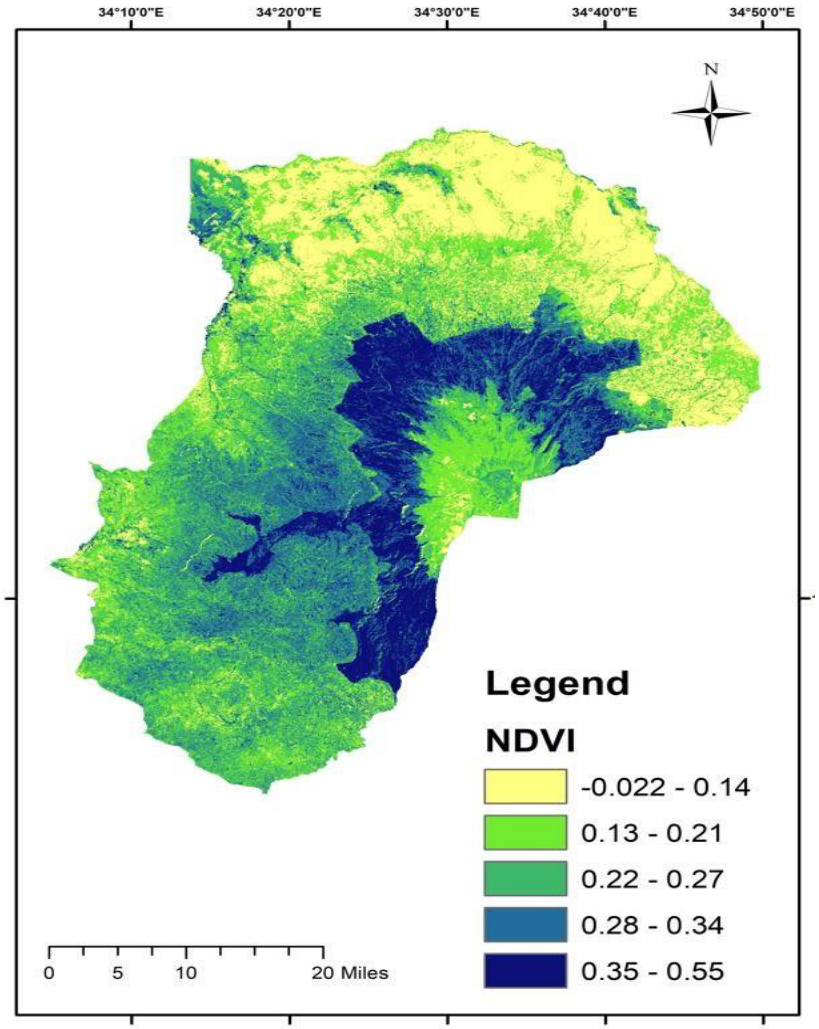

Figure 16: Map of Mount Elgon region showing Spatial distribution of NDVI.

4.4.1.9 Rainfall

From figure 17, rainfall plays a critical role in flood susceptibility given it's a primary conditioning factor of flood events (IPCC, 2021). Based on the rainfall analysis for this study, the results were categorized into distinct classes based on the magnitude of annual rainfall. The classification ranges from Very Low to Very High. Climate thresholds for GIS based flood suitability mapping for this study included above 1,774mm as very high, 1641 -1773 as high, 1460 – 1640 as moderate, 1259 -1456 as low and 1060 mm – 1,257mm as very low as shown in Figure 17.

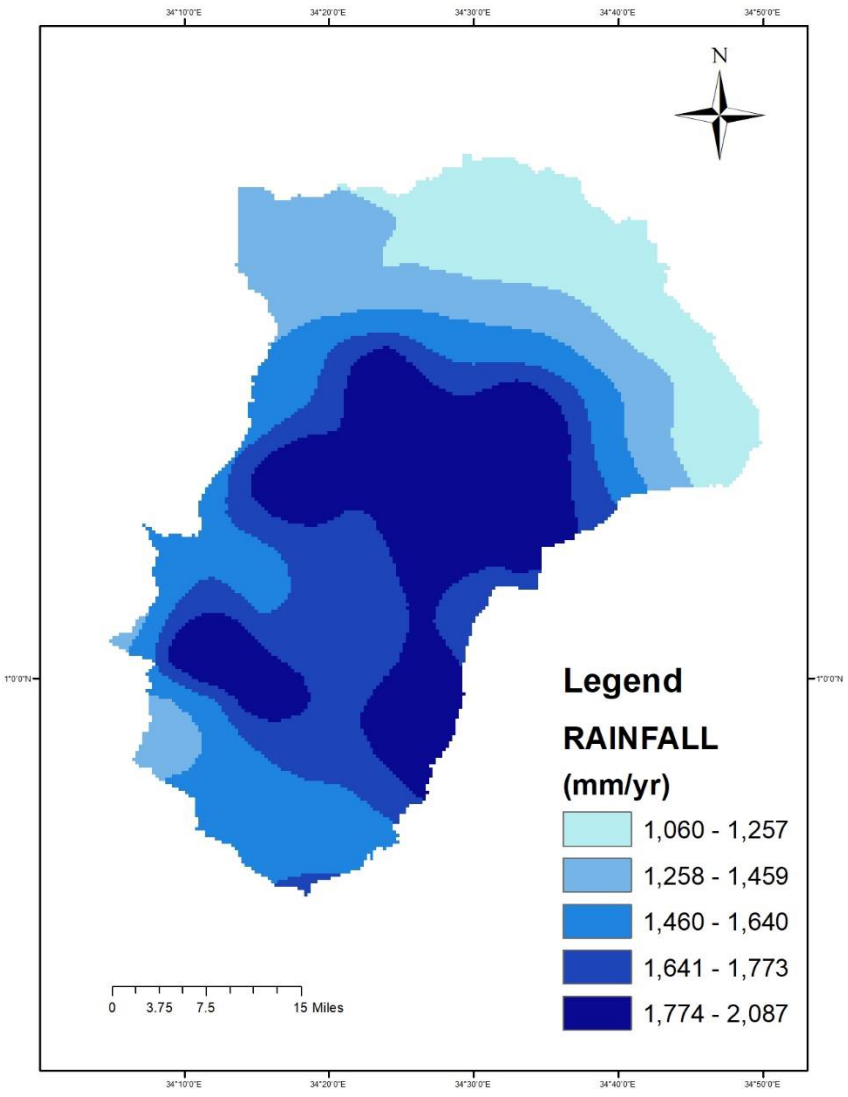

Figure 17: Map of Mount Elgon region showing Spatial distribution of rainfall.

4.4.1.10 Soil Type

Soil type is highly important indicating areas that are prone to flooding because it directly affects the drainage process because of the soil characteristics (Samanta et al., 2018). The study identified five soil types based on the FAO soil classifications scheme (figure 18). These include sandy clay loam, clay loam, grey clay, sandy grey and brown clay soils.

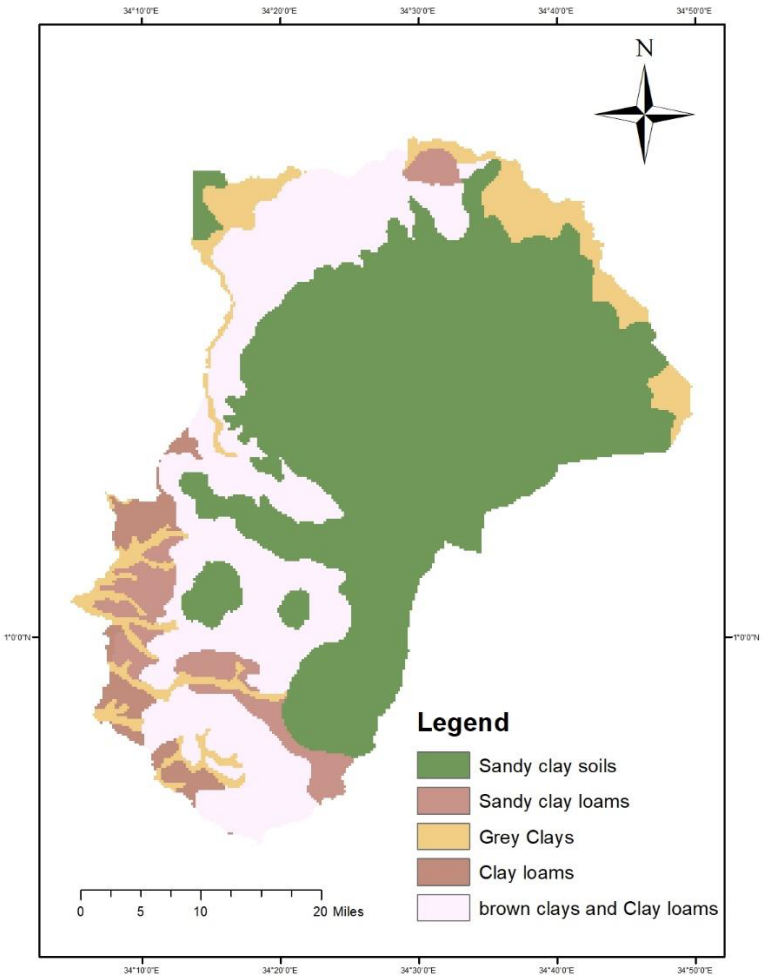

Figure 18: Map of Mount Elgon region showing Spatial distribution of soil type.

4.4.2 Analytical Hierarchy Process Modeling

The AHP modeling generated a Consistency Ration (CR) of 0.046 was obtained which is less than 0.1 which confirmed that the expert opinions provided consistent and reliable judgment in the AHP process.

Table 8: AHP Modelling results

		TWI	Elevation	Slope	Rainfall	LULC	NDVI	Distance from the river	Distance from the road	Drainage density	Soil type	Normalized principle Eigen
		1	2	3	4	5	6	7	8	9	10	
TWI	1	1	1	2	1	3	5	1	5	1	4	16%
Elevation	2	1	1	1	2	3	1	0.33	3	1	3	10%
Slope	3	0.50	1	1	0.25	2	2	0.50	2	1	4	8%
Rainfall	4	1	5	4	1	5	5	3	5	2	4	25%
LULC	5	0.33	0.33	0.50	0.20	1	1	0.50	1	1	2	5%
NDVI	6	0.20	1	0.50	0.20	1	1	0.33	2	0.33	1	4%
Distance from river	7	1	3	2	0.33	2	3	1	5	1	4	14%
Distance from road	8	0.2	0.33	0.50	0.20	1	0.50	0.20	1	0.33	3	4%
Drainage density	9	1	1	1	0.5	1	3	1	3	1	3	10%
Soil type	10	0.23	0.33	0.25	0.25	0.50	1	0.33	0.33	1		4%

As illustrated in Table 8, the results reveal that rainfall, distance from the river, and TWI are most influential factors determining flood susceptibility in the Mount Elgon region. Rainfall factor with 25% indicates that areas with elevated rainfall amount are prone to frequent and severe flooding. Distance from the river had a weighting of 14% suggesting that proximity to rivers significantly influenced flood susceptibility, the influence of topography on flooding had a weighting of 16%, implying that TWI has a greater influence on flooding compared to the other conditioning factors.

4.4.3 Weighted Overlay

The conditioning factors were overlaid based on the assigned weighed generated from the AHP model (Table 8).

Figure 19 illustrates that rainfall has the greatest influence, followed by TWI, distance from the river, drainage density, elevation, slope, land use and land cover (LULC), NDVI, distance from the road, and lastly, soil type.

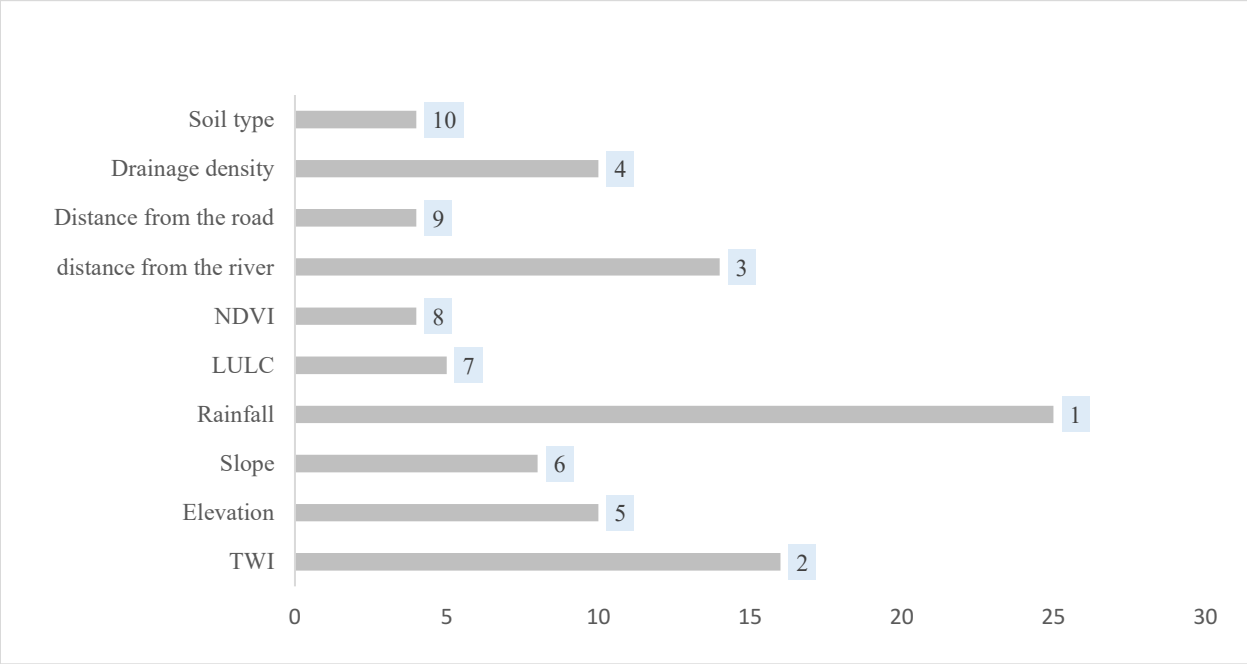

Figure 19: A graph showing weighted overlay ranks (labeled in blue) for each conditioning factor

The overlay tool assigned the score to each pixel of the Mount Elgon region with high scores indicated areas with high susceptibility to floods while low scores indicated areas less prone to flooding. Susceptibility map was generated representing the total area in square kilometers prone to the corresponding response unit as shown in figure 20. The area of mount Elgon that is moderately susceptible to flooding is approximately 900 sq.km (Table 9) and the area that is highly susceptible to flooding is approximately 2 sq.km (Table 9). Collectively, these areas are mostly located in the low lands where accumulation of rainfall occurs.

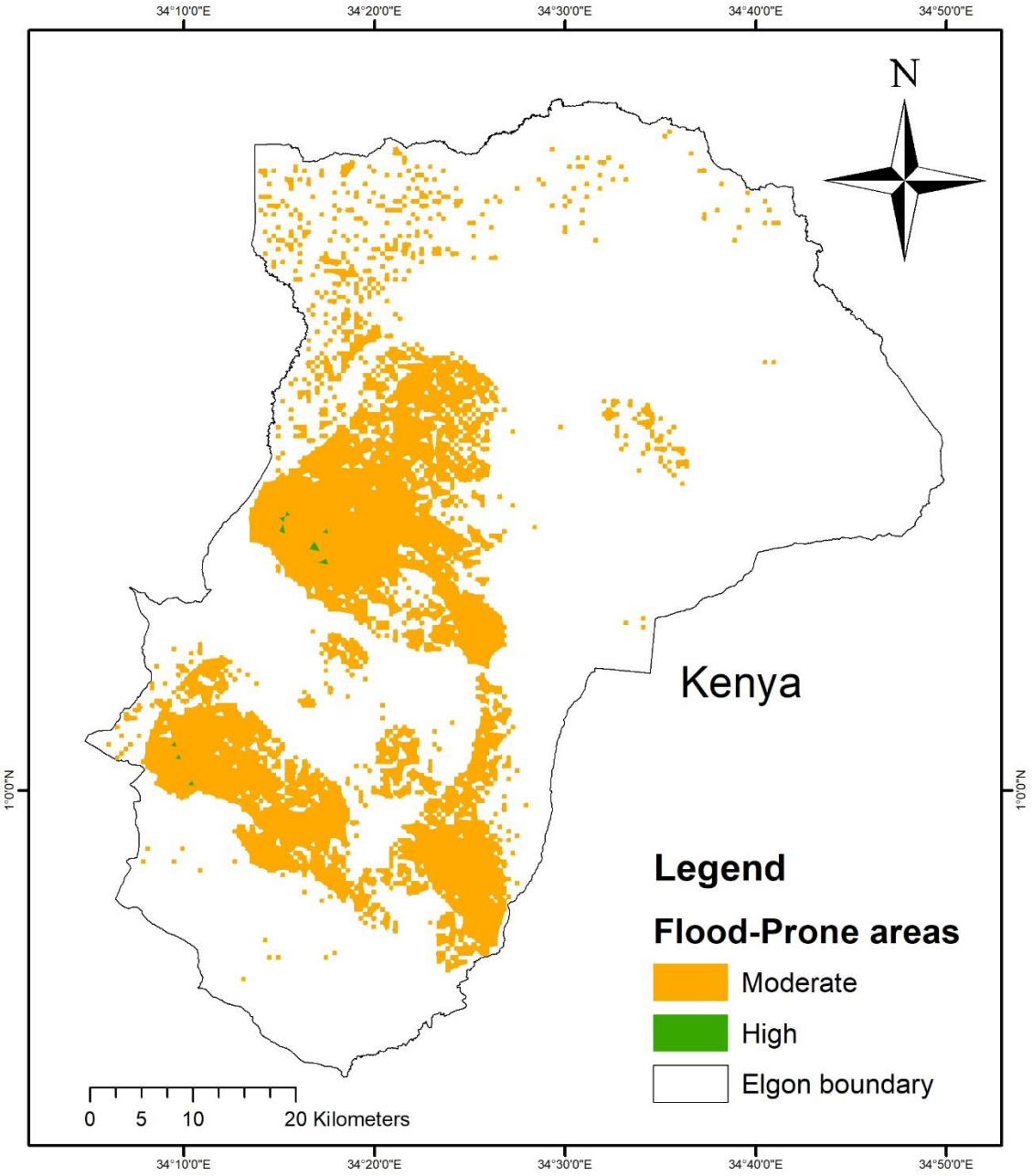

Figure 20: A map showing current flood susceptibility map in mount elgon region showing moderate to high flood susceptible areas.

Table 9: Area in Sq.km that is currently susceptible to flooding

Response Units	Total area in Sq.km
Moderate	821
High	1.6

4.5 Future Flood Susceptibility

To predict and map the flood susceptibility of the Elgon region under a changing climate scenario, the rainfall layer in the GIS model used in 4.3 above was replaced with the climate change scenario rainfall layer, then the rainfall layer was weighted along with other conditioning factors. The susceptibility was generated in the period of 2030 to 2050 across the scenarios that included RCP 2.6, RCP 4.5 (median global emission scenario), and RCP 8.5 (high global emission scenario) as shown in Figure 16 (low emission scenario). Finally, the area of each response unit in each climate scenario were calculated and represented in table 10.

As illustrated in Figure 21, the derived flood susceptibility showed that under RCP 2.6, most of the North, North Eastern and parts of the Elgon region is likely to become prone to floods with an area of about 9.2 square kilometers being highly flood susceptible and an area of 153.53 square kilometers will be very highly susceptible to flood during the 2030 to 2050 period. The climate scenario of RCP 4.5 indicated the same response classes of high and very high. An area of about 9.01 sq.km highly affected by flood and about 148.29 sq.km very highly affected by flood. Finally, scenario RCP 8.5 showed the same classes of changes as 2.6 and 4.5 with about 9.28 Sq.km highly susceptible to flooding and 154.67 very highly prone to flooding. The study observed a slight increase in the area that are highly susceptible to flooding as compared to scenario RCP 4.5.

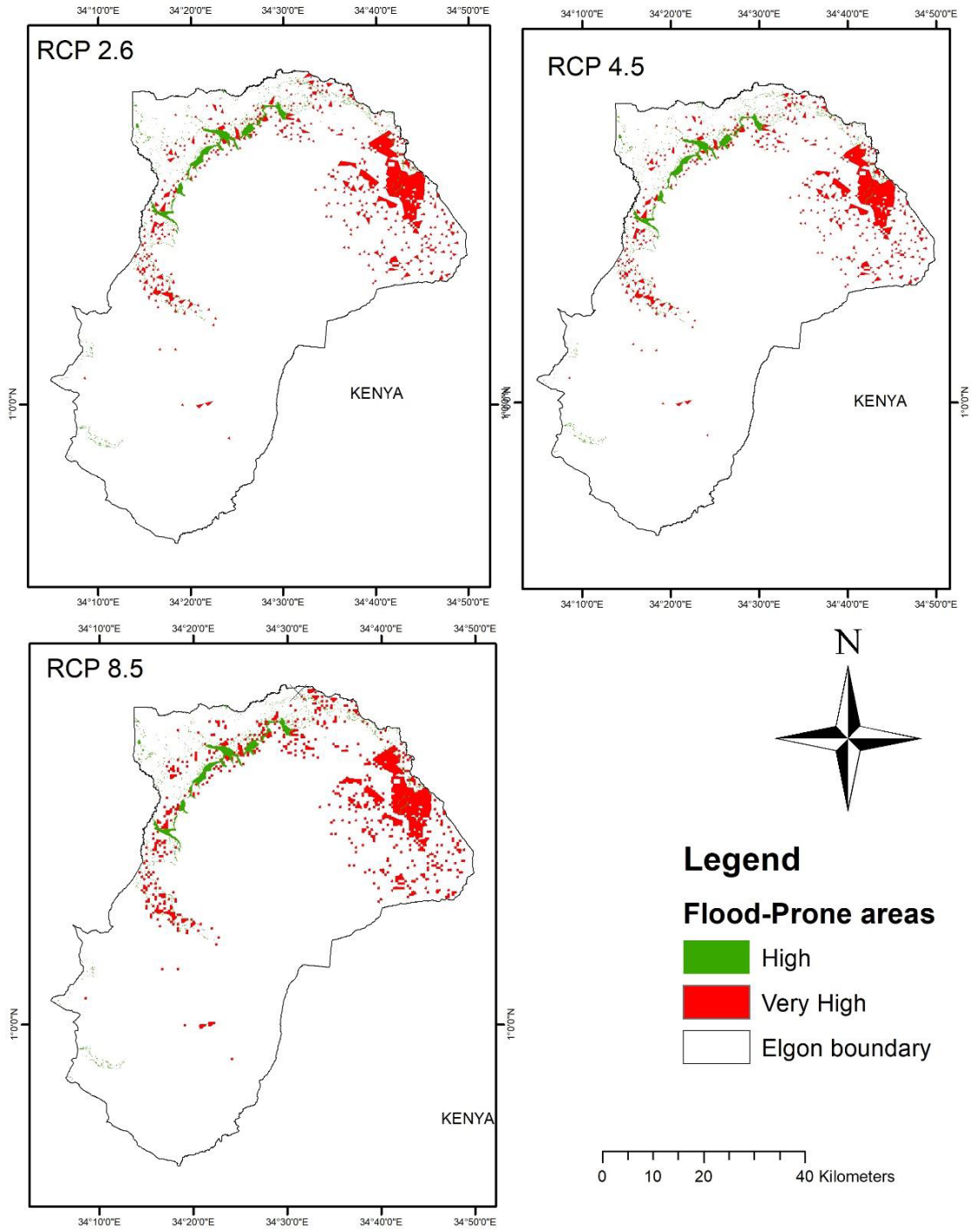

Figure 21: The flood susceptibility maps of the Elgon region in 2030 -2050 under three climate change scenarios.

Comparing the area of flood susceptibility classes in all the scenarios to the current flood susceptibility in section 4.3, the study concluded that the Elgon region flood susceptibility ranged from moderate to very high in all analyzed climate excluding the low and very low. This showed

that the region experiences high floods (Resilience, 2010). The current flood susceptible areas range from moderate to high. High flood susceptible areas increase across all the RCP scenarios and areas located in the lowlands which are the catchment areas of mount Elgon are likely to become very highly susceptible to flooding events in the year 2030 to 2050.

Overall, it's clear that the flood susceptibility is expected to increase under the RCP 2.6, RCP 4.5, and RCP 8.5 scenarios for both High and Very High flood susceptibility levels compared to the "Current" scenario. This clearly shows that climate change will bring about increase in rainfall which will change the areas susceptible to flood.

Table 10: A comparison area in Sq.km of current and future climate scenarios (RCP 2.6, RCP 4.5, and RCP 8.5) that is susceptible to floods.

Flood susceptibility Response units	Current flood prone area (Km^2)	RCP 2.6 flood prone area (Km^2)	RCP 4.5 flood prone area (Km^2)	RCP 8.5 flood prone area (Km^2)
Moderate	821	0	0	0
High	1.6	9.2	9.01	9.28
Very High	0	153.63	148.63	154.67

4.6 Impacts of Projected Floods on the Farmland Food Security

The study observed that under RCP 2.6 (figure 22), most of the farmlands in the south of the Elgon region will not be affected by the floods however, the high flood prone farmlands are located in the northern areas around Bukwo district with and approximate area of 128 square kilometers highly affected.

Similarity, under RCP 4.5, the farmlands that are likely to be exposed and prone to very high flooding lie in the northern area of the region in places around Bukwo district, the total farmland area that will be affected under this scenario is around 118.5 sq.km for both high and very high flood response units as shown in Table 11.

Table 11: Farmland Area Exposed to Future Flood Susceptibility under Different Climate Change Scenarios (RCP 2.6, RCP 4.5, RCP 8.5).

	Farmland area exposed under RCP 2.6 (Km^2)	Farmland area exposed under RCP 4.5(Km^2)	Farmland area exposed under RCP 8.5(Km^2)
High	3.8	3.5	4.0
Very High	127	115	131

Lastly, under RCP 8.5 as shown in Figure 22, this study observed that there is an increase in the area of the farm land affected by floods. Furthermore, there is an increase in the farmland area affected by flood under this climate change scenario.

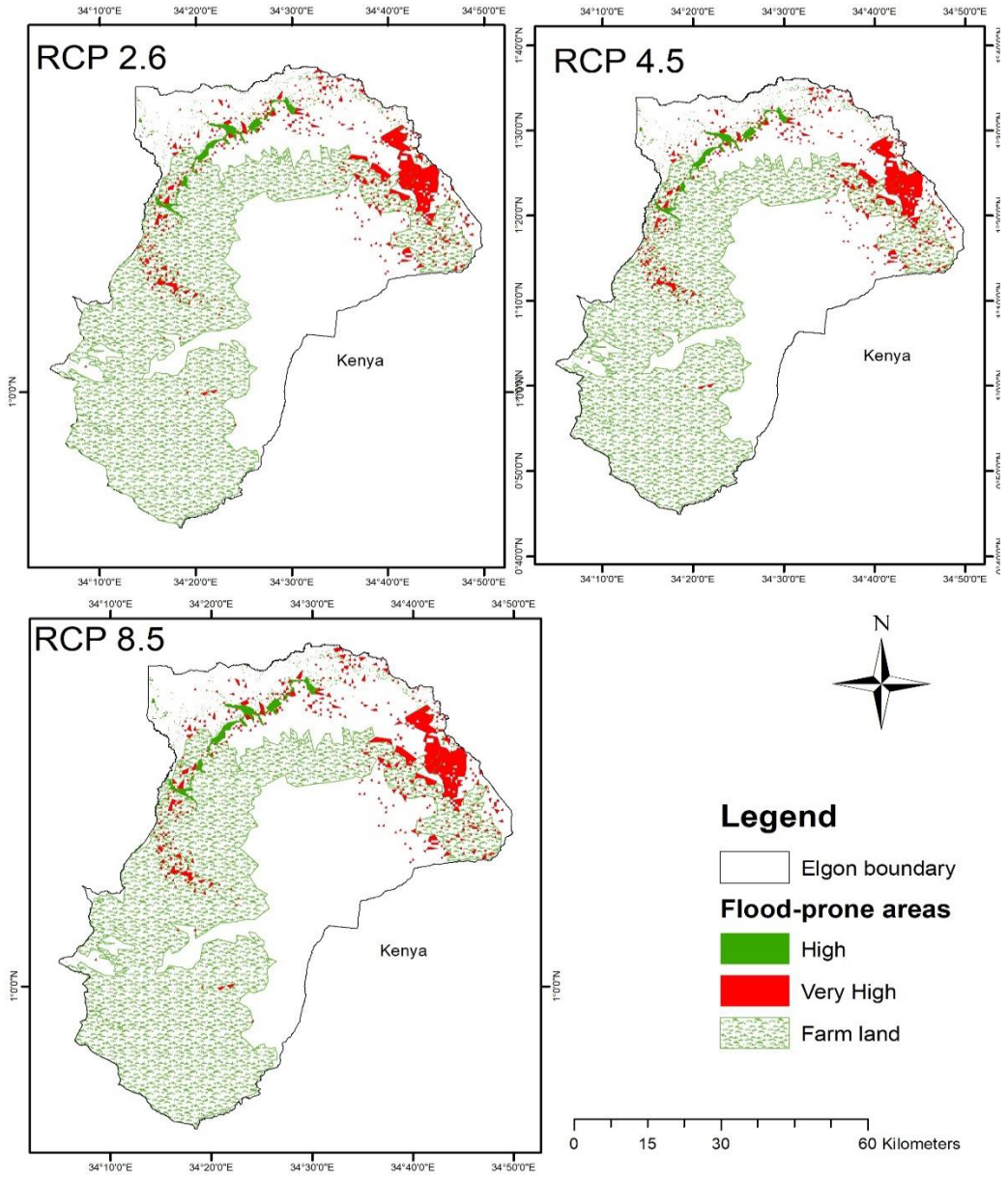

Figure 22: The flood impact maps on the Farmlands of the Elgon region in the years 2030 -2050 under three climate change scenarios.

Over all, there is no significant changes in the areas of farmlands affected by flood in among the three climate scenarios. However, all scenarios showed that the farmlands in the northern part of the study domain, particularly in Bukwo and bulambuli district will be the most affected for the period of 2030 to 2050. This is attributed to the significant trend and positive increase in rainfall received in that region especially in the MAM season as shown in section 4.3.1. This therefore concludes that climate change poses additional challenges to farmland and food security in general.

CHAPTER FIVE

CONCLUSIONS AND RECOMMENDATIONS

5.1 Conclusions

The study has successfully examined flood susceptibility in the Mount Elgon region over the period of 1991 to 2022. The analysis of seasonal rainfall patterns identified significant trends, as indicated by Z, S, and P values, highlighting the likelihood of increased flood risks in specific seasons and observation points.

To examine the spatial distribution of flood susceptibility, the study concludes that rainfall, distance from the river, and topographic wetness index were the most influencing conditional factors and the flood susceptibility map, indicated moderate and high flood-prone areas primarily in the North region of the study area.

Furthermore, the study projected future flood susceptibility under different climate change scenarios (RCP 2.6, RCP 4.5, RCP 8.5). The study concluded that there is an increasing trend in highly flood-prone areas, in line with observed intensifying rainfall trends.

The potential impact of projected floods on the agricultural sector, a vital component of food security, was also assessed. Results highlighted the vulnerability of farmlands in the northern areas, particularly around Bukwo district, to flooding, posing potential disruptions to agricultural activities and food production.

In response to the stated objectives, this study successfully examined seasonal precipitation patterns, determined current flood susceptibility characteristics, predicted future flood-susceptible areas, and assessed the implication of projected floods on farmland food security. The finding in the study suggest that there are changes in the flood-susceptible areas in the Elgon region of Uganda and its implication to food security are evident.

5.2 Recommendations

This section indicates recommendations generated from the results to planners and scientist.

5.2.1 Recommendations to Planners

The findings of this study are intended to inform and guide the planners in key ways of

- Policy maker should use this data to implement more effective and targeted early warning systems, land use planning, and infrastructure planning and investment.
- Policy makers should use this information from this study to put in place necessary contingency measures to build community resilience programs as well as develop and climate change adaptation strategies.
- The planners can also use the flood susceptibility information from this study to empower farmers to navigate the changing flood patterns and devise agricultural practices to cope with the changes.

5.2.2 Recommendations to Scientists

- Given the dynamic nature of climate patterns and flood susceptibility, scientists should continue monitoring and researching the Mount Elgon region while refining the models.
- The study recommends future studies to be done on analyzing the seasonal flood susceptibility both for the current and future climate scenarios in Elgon region as it is necessary for the farmers.
- Scientists should as well conduct in-depth studies that model the impact of various flood scenarios on agricultural systems for example transportation and crop types so as to insights crucial for devising scenario-specific strategies to mitigate flood insecurity.

REFERENCES

Adhikari, S., Caron, L., Steinberger, B., Reager, J. T., Kjeldsen, K. K., Marzeion, B., Larour, E., & Ivins, E. R. (2018). Methods 1. *Earth and Planetary Science Letters*, *502*(1), suppl.

Aditya, F., Gusmayanti, E., & Sudrajat, J. (2021). Rainfall trend analysis using Mann-Kendall and Sen's slope estimator test in West Kalimantan. *IOP Conference Series: Earth and Environmental Science*, *893*(1). https://doi.org/10.1088/1755-1315/893/1/012006

Adnan, M. S. G., Abdullah, A. Y. M., Dewan, A., & Hall, J. W. (2020). The effects of changing land use and flood hazard on poverty in coastal Bangladesh. *Land Use Policy*, *99*(May), 104868. https://doi.org/10.1016/j.landusepol.2020.104868

Akdeniz, H. B., Sag, N. S., & Inam, S. (2023). Analysis of land use/land cover changes and prediction of future changes with land change modeler: Case of Belek, Turkey. *Environmental Monitoring and Assessment*, *195*(1), 1–28. https://doi.org/10.1007/s10661-022-10746-w

Alashan, S. (2020). Combination of modified Mann-Kendall method and Şen innovative trend analysis. *Engineering Reports*, *2*(3), 1–13. https://doi.org/10.1002/eng2.12131

Albano, R., & Sole, A. (2018). Geospatial methods and tools for natural risk management and communications. *ISPRS International Journal of Geo-Information*, *7*(12). https://doi.org/10.3390/ijgi7120470

Aswad, F., Yousif, A., & Ibrahim, S. (2020). Trend Analysis Using Mann-kendall And Sen's Slope Estimator Test for Annual And Monthly Rainfall for Sinjar District, Iraq. *The Journal of the University of Duhok*, *23*(2), 501–508. https://doi.org/10.26682/csjuod.2020.23.2.41

Balgah, R. A., Ngwa, K. A., Buchenrieder, G. R., & Kimengsi, J. N. (2023). Impacts of Floods on Agriculture-Dependent Livelihoods in Sub-Saharan Africa: An Assessment from Multiple Geo-Ecological Zones. *Land*, *12*(2). https://doi.org/10.3390/land12020334

Basheer, S., Wang, X., Farooque, A. A., Nawaz, R. A., Liu, K., Adekanmbi, T., & Liu, S. (2022). Comparison of Land Use Land Cover Classifiers Using Different Satellite Imagery and Machine Learning Techniques. *Remote Sensing*, *14*(19), 1–18. https://doi.org/10.3390/rs14194978

Bonzemo, S. B. (2018). To Examine Coping Adaptive Strategies Used by Households and Make Policy Recommendations for Addressing Future Climate Change Impacts on Livelihoods in Kapsokwony Division, Mt. Elgon Sub-County, Bungoma County, Kenya. *International Journal of Educational Studies*, *1*(4), 251–269. https://doi.org/10.53935/2641-533x.v1i4.94

Buchecker, M., Salvini, G., Di Baldassarre, G., Semenzin, E., Maidl, E., & Marcomini, A. (2013). The role of risk perception in making flood risk management more effective. *Natural Hazards and Earth System Sciences*, *13*(11), 3013–3030. https://doi.org/10.5194/nhess-13-3013-2013

Chau, V. N., Holland, J., Cassells, S., & Tuohy, M. (2013). Using GIS to map impacts upon agriculture from extreme floods in Vietnam. *Applied Geography*, *41*, 65–74. https://doi.org/10.1016/j.apgeog.2013.03.014

Chen, Y. J., Lin, H. J., Liou, J. J., Cheng, C. T., & Chen, Y. M. (2022). Assessment of Flood Risk Map under Climate Change RCP8.5 Scenarios in Taiwan. *Water (Switzerland)*, *14*(2), 1–17. https://doi.org/10.3390/w14020207

Ciscar, J. C., Paci, D., & Vergano, L. (2010). Issues on the economics of adaptation to climate change. *Climate Change Policies: Global Challenges and Future Prospects*, 29–49. https://doi.org/10.4337/9781781000885.00012

Costache, R. (2020). Using GIS , Remote Sensing , and Machine Learning to Highlight the Correlation between the. *Remote Sensing*, *12*.

Crawford, A., Price-Kelly, H., Terton, A., & Echeverría, D. (2016). Review of current and planned adaptation action in Burkina Faso. 55), 3(*4*, □□□□□ □□□□□. https://idl-bnc-idrc.dspacedirect.org/handle/10625/55876

Dankers, R., & Feyen, L. (2009). Flood hazard in Europe in an ensemble of regional climate scenarios. *Journal of Geophysical Research Atmospheres*, *114*(16), 47–62. https://doi.org/10.1029/2008JD011523

Dede, M., Asdak, C., & Setiawan, I. (2022). Spatial dynamics model of land use and land cover changes: A comparison of CA, ANN, and ANN-CA. *Register: Jurnal Ilmiah Teknologi Sistem Informasi*, *8*(1), 38–49. https://doi.org/10.26594/register.v8i1.2339

Devereux, S. (2007). The impact of droughts and floods on food security and policy options to alleviate negative effects. *Agricultural Economics*, *37*(S1), 47–58. https://doi.org/10.1111/j.1574-0862.2007.00234.x

Di Baldassarre, G., Montanari, A., Lins, H., Koutsoyiannis, D., Brandimarte, L., & Blschl, G. (2010). Flood fatalities in Africa: From diagnosis to mitigation. *Geophysical Research Letters*, *37*(22), 2–6. https://doi.org/10.1029/2010GL045467

Duan, Y., Xiong, J., Cheng, W., Li, Y., Wang, N., Shen, G., & Yang, J. (2022). Increasing Global Flood Risk in

2005–2020 from a Multi-Scale Perspective. *Remote Sensing*, *14*(21). https://doi.org/10.3390/rs14215551

Eckstein, D., Künzel, V., & Schäfer, L. (2021). Global climate risk index 2021: who suffers most from extreme weather events? Weather-related loss events in 2019 and 2000–2019. In *Germanwatch* (Issue March). http://germanwatch.org/en/download/8551.pdf

Edamo, M. L., Bushira, K., & Ukumo, T. Y. (2022). Flood susceptibility mapping in the Bilate catchment, Ethiopia. *H2Open Journal*, *5*(4), 691–712. https://doi.org/10.2166/h2oj.2022.128

Ekeanyanwu, C. V., Bose, P., Beavers, M., Yuan, Y., & Obisakin, I. (2022). Modeling and Mapping Flood Hazard with a Flood Risk Assessment Tool: A Case Study of Austin, Texas. *Journal of Geographic Information System*, *14*(04), 332–346. https://doi.org/10.4236/jgis.2022.144018

El-Haddad, B. A., Youssef, A. M., Pourghasemi, H. R., Pradhan, B., El-Shater, A. H., & El-Khashab, M. H. (2021). Flood susceptibility prediction using four machine learning techniques and comparison of their performance at Wadi Qena Basin, Egypt. In *Natural Hazards* (Vol. 105, Issue 1). https://doi.org/10.1007/s11069-020-04296-y

Endris, H. S., Lennard, C., Hewitson, B., Dosio, A., Nikulin, G., & Artan, G. A. (2019). Future changes in rainfall associated with ENSO , IOD and changes in the mean state over Eastern Africa. *Climate Dynamics*, *52*(3), 2029–2053. https://doi.org/10.1007/s00382-018-4239-7

Findayani, A., Aji, A., Juhadi, M., & Indrayati, A. (2019). *Semarang City Food Risk Disaster Mapping Based on Geographic Information System*. *313*(ICoRSIA 2018), 311–313. https://doi.org/10.2991/icorsia-18.2019.74

Fischer, G., & Shah, M. (2010). *Farmland investments and food security*. *August*, 42.

Forte, F., Strobl, R. O., & Pennetta, L. (2006). A methodology using GIS, aerial photos and remote sensing for loss estimation and flood vulnerability analysis in the Supersano-Ruffano-Nociglia Graben, southern Italy. *Environmental Geology*, *50*(4), 581–594. https://doi.org/10.1007/s00254-006-0234-0

G.Ramakrishna, Solomon, R. G., & I. Daisy. (2014). Impact of Floods on Food Security and Livelihoods of Idp Tribal. *International Journal of Development and Economics Sustainability*, *2*(1), 11–24.

Gitz, V., Meybeck, A., Lipper, L., Young, C., & Braatz, S. (2016). Climate change and food security: Risks and responses. In *Food and Agriculture Organization of the United Nations*. https://doi.org/10.1080/14767058.2017.1347921

Hosseinzadeh, S. R. (2011). between the drainage network extracted automatically from a DEM and the network delineation from photographs and satellite Images comprises three steps: Drawing rivers from aerial photographs and satellite Images, automated delineation from an ASTER DEM b. *International Journal of Environmental Science and Development*, *2*(3).

IPCC. (2014). *the Ipcc'S Fifth Assessment Report (Ar5)*. *September 2013*.

IPCC. (2021). Climate Change 2021 The Physical Science Basis WGI. In *Bulletin of the Chinese Academy of Sciences* (Vol. 34, Issue 2).

Janizadeh, S., Avand, M., Jaafari, A., Van Phong, T., Bayat, M., Ahmadisharaf, E., Prakash, I., Pham, B. T., & Lee, S. (2019). Prediction success of machine learning methods for flash flood susceptibility mapping in the Tafresh watershed, Iran. *Sustainability (Switzerland)*, *11*(19), 1–19. https://doi.org/10.3390/su11195426

Jiang, B., Bamutaze, Y., & Pilesjö, P. (2014). Climate change and land degradation in Africa: A case study in the Mount Elgon region, Uganda. *Geo-Spatial Information Science*, *17*(1), 39–53. https://doi.org/10.1080/10095020.2014.889271

Kamaraj, M., & Rangarajan, S. (2022). Predicting the future land use and land cover changes for Bhavani basin, Tamil Nadu, India, using QGIS MOLUSCE plugin. *Environmental Science and Pollution Research*, *29*(57), 86337–86348. https://doi.org/10.1007/s11356-021-17904-6

Kansiime, M. K., Wambugu, S. K., & Shisanya, C. A. (2013a). Perceived and Actual Rainfall Trends and Variability in Eastern Uganda : Implications for Community Preparedness and Response. *Journal of Natural Sciences Research*, *3*(8), 179–195.

Kansiime, M. K., Wambugu, S. K., & Shisanya, C. A. (2013b). Perceived and Actual Rainfall Trends and Variability in Eastern Uganda. *Journal of Natural Sciences Research*, *3*(8), 179–195.

Karmakar, S., Simonovic, S. P., Peck, A., & Black, J. (2010). An Information System for Risk-Vulnerability Assessment to Flood. *Journal of Geographic Information System*, *02*(03), 129–146. https://doi.org/10.4236/jgis.2010.23020

Kim, N. W., Lee, J. Y., Park, D. H., & Kim, T. W. (2019). Evaluation of future flood risk according to rcp scenarios using a regional flood frequency analysis for ungauged watersheds. *Water (Switzerland)*, *11*(5). https://doi.org/10.3390/w11050992

Kundzewicz, Z. W., & Schellnhuber, H. J. (2004). Floods in the IPCC TAR perspective. *Natural Hazards*, *31*(1), 111–128. https://doi.org/10.1023/B:NHAZ.0000020257.09228.7b

Kundzewicz, Zbigniew W., Kanae, S., Seneviratne, S. I., Handmer, J., Nicholls, N., Peduzzi, P., Mechler, R., Bouwer, L. M., Arnell, N., Mach, K., Muir-Wood, R., Brakenridge, G. R., Kron, W., Benito, G., Honda, Y., Takahashi, K., & Sherstyukov, B. (2014). Le risque d'inondation et les perspectives de changement climatique mondial et régional. *Hydrological Sciences Journal*, *59*(1), 1–28. https://doi.org/10.1080/02626667.2013.857411

Lashkari, H., & Jafari, M. (2021). Annual displacement and appropriate index to determine ITCZ position in East Africa and the Indian Ocean regions. *Meteorology and Atmospheric Physics*, *Scott 2013*. https://doi.org/10.1007/s00703-021-00797-y

McKinney, L., & Wright, D. C. (2021). Climate change and water dynamics in rural Uganda. *Sustainability (Switzerland)*, *13*(15), 12–14. https://doi.org/10.3390/su13158322

Milly, P. C. D., Wetherald, R. T., Dunne, K. A., & Delworth, T. L. (2002). Increasing risk of great floods in a changing climate. *Nature*, *415*(6871), 514–517. https://doi.org/10.1038/415514a

Montz, B. E., & Evans, T. A. (2001). Gis and Social Vulnerability Analysis. *Coping With Flash Floods*, 37–48. https://doi.org/10.1007/978-94-010-0918-8_5

Muhammad, R., Zhang, W., Abbas, Z., Guo, F., & Gwiazdzinski, L. (2022). Spatiotemporal Change Analysis and Prediction of Future Land Use and Land Cover Changes Using QGIS MOLUSCE Plugin. *Mdpi*. https://www.mdpi.com/2073-445X/11/3/419/htm

Nakileza, B. R., & Mugagga, F. (2022). *Assessment of Landslide susceptibility and risk to road network in Mt Elgon , Uganda*. 1–25.

Ngoma, H., Wen, W., Ayugi, B., Karim, R., & Makula, E. K. (2021). Mechanisms associated with September to November (SON) rainfall over Uganda during the recent decades. *Geographica Pannonica*, *25*(1), 10–23. https://doi.org/10.5937/gp25-29932

O'Donnell, E. C., & Thorne, C. R. (2020). Drivers of future urban flood risk. *Philosophical Transactions of the Royal Society A: Mathematical, Physical and Engineering Sciences*, *378*(2168). https://doi.org/10.1098/rsta.2019.0216

Obubu, J. P., Mengistou, S., Fetahi, T., Alamirew, T., Odong, R., & Ekwacu, S. (2021). Recent climate change in the lake kyoga basin, Uganda: An analysis using short-term and long-term data with standardized precipitation and anomaly indexes. *Climate*, *9*(12). https://doi.org/10.3390/cli9120179

Ogania, J. L., Puno, G. R., Alivio, M. B. T., & Taylaran, J. M. G. (2019). Effect of digital elevation model's

resolution in producing flood hazard maps. *Global Journal of Environmental Science and Management*, *5*(1), 95–106. https://doi.org/10.22034/gjesm.2019.01.08

Onyutha, C., Asiimwe, A., Ayugi, B., Ngoma, H., Ongoma, V., & Tabari, H. (2021). Observed and future precipitation and evapotranspiration in water management zones of uganda: Cmip6 projections. *Atmosphere*, *12*(7), 1–25. https://doi.org/10.3390/atmos12070887

OPM. (2020). *NATIONAL RISK AND VULNERABILITY of Uganda*.

Palmer, P. I., Wainwright, C. M., Dong, B., Maidment, R. I., Wheeler, K. G., Gedney, N., Hickman, J. E., Madani, N., Folwell, S. S., Abdo, G., Allan, R. P., Black, E. C. L., Feng, L., Gudoshava, M., Haines, K., Huntingford, C., Kilavi, M., Lunt, M. F., Shaaban, A., & Turner, A. G. (2023). *Drivers and impacts of Eastern African rainfall variability*. *4*(April). https://doi.org/10.1038/s43017-023-00397-x

Papalexiou, S. M., & Montanari, A. (2019). Global and Regional Increase of Precipitation Extremes Under Global Warming. *Water Resources Research*, *55*(6), 4901–4914. https://doi.org/10.1029/2018WR024067

Pinstrup-Andersen, P. (2009). Food security: definition and measurement. *Food Security*, *1*(1), 5–7. https://doi.org/10.1007/s12571-008-0002-y

Pourali, S. H., Arrowsmith, C., Chrisman, N., Matkan, A. A., & Mitchell, D. (2016). Topography Wetness Index Application in Flood-Risk-Based Land Use Planning. *Applied Spatial Analysis and Policy*, *9*(1), 39–54. https://doi.org/10.1007/s12061-014-9130-2

Rahman, M., Ningsheng, C., Mahmud, G. I., Islam, M. M., Pourghasemi, H. R., Ahmad, H., Habumugisha, J. M., Washakh, R. M. A., Alam, M., Liu, E., Han, Z., Ni, H., Shufeng, T., & Dewan, A. (2021). Flooding and its relationship with land cover change, population growth, and road density. *Geoscience Frontiers*, *12*(6), 101224. https://doi.org/10.1016/j.gsf.2021.101224

Reed, C., Anderson, W., Kruczkiewicz, A., Nakamura, J., Gallo, D., Seager, R., & McDermid, S. S. (2022). The impact of flooding on food security across Africa. *Proceedings of the National Academy of Sciences of the United States of America*, *119*(43). https://doi.org/10.1073/pnas.2119399119

Rentschler, J., Salhab, M., & Jafino, B. A. (2022). Flood exposure and poverty in 188 countries. *Nature Communications*, *13*(1), 1–11. https://doi.org/10.1038/s41467-022-30727-4

Resilience, B. C. (2010). *Climate Change in Uganda Insights for Long term Adaptation and*. *July*.

Ripple, W. J., Wolf, C., Newsome, T. M., Gregg, J. W., Lenton, T. M., Palomo, I., Eikelboom, J. A. J., Law, B. E., Huq, S., Duffy, P. B., & Rockström, J. (2021). World scientists' warning of a climate emergency

2021. *BioScience*, *71*(9), 894–898. https://doi.org/10.1093/biosci/biab079

Ro, R. (2001). GIS and geostatistics: Essential partners for spatial analysis. *Environmental and Ecological Statistics*, *8*.

Rocha, J., Duarte, A., Silva, M., Fabres, S., Vasques, J., Revilla-Romero, B., & Quintela, A. (2020). The importance of high resolution digital elevation models for improved hydrological simulations of a mediterranean forested catchment. *Remote Sensing*, *12*(20), 1–17. https://doi.org/10.3390/rs12203287

Roopnarine, R., Opadeyi, J., Eudoxie, G., Thongs, G., & Edwards, E. (2018). GIS-based Flood Susceptibility and Risk Mapping Trinidad Using Weight Factor Modeling. *Caribbean Journal of Earth Science*, *49*(August), 1–9.

Roy, S., & Chakravarty, N. (2021). *Rainfall Analysis by Using Mann-Kendall Trend, Sen's Slope and Variability at Six Stations of Andaman & Nicobar Islands*.

Saaty, R. W. (1987). The analytic hierarchy process-what it is and how it is used. *Mathematical Modelling*, *9*(3–5), 161–176. https://doi.org/10.1016/0270-0255(87)90473-8

Samanta, S., Pal, D. K., & Palsamanta, B. (2018). Flood susceptibility analysis through remote sensing, GIS and frequency ratio model. *Applied Water Science*, *8*(2), 1–14. https://doi.org/10.1007/s13201-018-0710-1

Shaw, D. J. (2007). *World Food Summit, 1996*. *May 1994*, 347–348.

SHIFIDI, V. T. (2016). Impact of flooding on rural livelihoods of the Cuvelai Basin in Northern Namibia. *Journal of Geography and Regional Planning*, *9*(6), 104–121. https://doi.org/10.5897/jgrp2015.0536

Simonović, S. P. (2009). Floods in a changing climate: Risk management. *Floods in a Changing Climate: Risk Management*, *2*, 1–179. https://doi.org/10.1017/CBO9781139088404

Tabari, H. (2020). Climate change impact on flood and extreme precipitation increases with water availability. *Scientific Reports*, *10*(1), 1–10. https://doi.org/10.1038/s41598-020-70816-2

Tariq, A., Yan, J., Ghaffar, B., Qin, S., Mousa, B. G., Sharifi, A., Huq, M. E., & Aslam, M. (2022). Flash Flood Susceptibility Assessment and Zonation by Integrating Analytic Hierarchy Process and Frequency Ratio Model with Diverse Spatial Data. *Water (Switzerland)*, *14*(19). https://doi.org/10.3390/w14193069

UBOS-Statistical Abstract. (2020). UGANDA BUREAU OF STATISTICS, 2020 Statistical Abstract. *Uganda*

Bureau of Statistics, *1*, 303. http://www.ubos.org/onlinefiles/uploads/ubos/pdf documents/abstracts/Statistical Abstract 2013.pdf

Uganda Investment Authority. (2019). *Elgon investment profile 2018*. https://www.ugandainvest.go.ug/wp-content/uploads/2019/06/Elgon-Investment-Profile.pdf

Umaru, E. T., & Adedokun, A. (2020). Geospatial Analysis of Flood Risk and Vulnerability Assessment along River Benue Basin of Kogi State. *Journal of Geographic Information System*, *12*(01), 1–14. https://doi.org/10.4236/jgis.2020.121001

UNFCC. (2021). *ANNEX I - UNDRR 2020 ANNUAL REPORT Progress against output indicators Strengthen Global Monitoring , Analysis and Coordination of Sendai Framework Implementation*. 1–20.

Uribe, Álvarez, M. C., Estrada Restrepo, A., Summit, U. N., Shamah-Levy, T., Mundo-Rosas, V., Rivera-Dommarco, J. A., S.E.D., C., A.G., P., O.F., H., Rose, D. D., Norhasmah, S., Zalilah, M. ., Asnarulkhadi, a. ., Larsen, A. F., Lilleør, H. B., Mundo-Rosas, J. A. G. de S., Kimani-Murage, E. W., Holding, P. a., Fotso, J.-C., … Afolabi, O. T. (2010). Ecuador y Bolivia son casos excepcionales en reducción de inseguridad alimentaria en la región. *Social Indicators Research*, *95*(1), 215–230. http://www.ncbi.nlm.nih.gov/pubmed/21812205%5Cnhttp://jn.nutrition.org/content/140/1/153S.abstract%5Cnhttp://link.springer.com/10.1007/s11205-009-9455-4%5Cnhttp://www.fao.org/docrep/013/al936e/al936e00.pdf%5Cnwww.andes.info.ec/es/noticias/fao-ecuador-boli

Wakachala, F. M., Shilenje, Z. W., Nguyo, J., Shaka, S., & Apondo, W. (2015). *Statistical Patterns of Rainfall Variability in the Great Rift Valley of Kenya Statistical Patterns of Rainfall Variability in the Great Rift Valley of Kenya*. *October*.

Ward, P. J., Jongman, B., Weiland, F. S., Bouwman, A., Van Beek, R., Bierkens, M. F. P., Ligtvoet, W., & Winsemius, H. C. (2013). Assessing flood risk at the global scale: Model setup, results, and sensitivity. *Environmental Research Letters*, *8*(4). https://doi.org/10.1088/1748-9326/8/4/044019

WBG. (2021). Climate Risk Country Profile: Uganda. *The World Bank Group*, 36. www.worldbank.org

Week, D. A., & Wizor, C. H. (2020). Effects of Flood on Food Security, Livelihood and Socio-economic Characteristics in the Flood-prone Areas of the Core Niger Delta, Nigeria. *Asian Journal of Geographical Research*, *January*, 1–17. https://doi.org/10.9734/ajgr/2020/v3i130096

Weldegebriel, Z. B., & Amphune, B. E. (2017). Livelihood resilience in the face of recurring floods: an empirical evidence from Northwest Ethiopia. *Geoenvironmental Disasters*, *4*(1), 1–19. https://doi.org/10.1186/s40677-017-0074-0

Wright, D. (1994). Methods in Flood Hazard and Risk Management. *International Bank for Reconstruction and Development / The World Bank*, *2*, 2–4.

Yamazaki, D., Watanabe, S., & Hirabayashi, Y. (2018). Global Flood Risk Modeling and Projections of Climate Change Impacts. *Geophysical Monograph Series*, *233*, 185–203. https://doi.org/10.1002/9781119217886.ch11

Zehra, S., & Afsar, S. (2016). Flood Hazard Mapping of Lower Indus Basin Using Multi-Criteria Analysis. *Journal of Geoscience and Environment Protection*, *04*(04), 54–62. https://doi.org/10.4236/gep.2016.44008

Zhang, L., Ameca, E. I., Cowlishaw, G., Pettorelli, N., Foden, W., & Mace, G. M. (2019). Global assessment of primate vulnerability to extreme climatic events. *Nature Climate Change*, *9*(7), 554–561. https://doi.org/10.1038/s41558-019-0508-7